

Redshift space distortions in the presence of non-minimally coupled dark matter

Fabio Chibana,¹ Rampei Kimura,² Masahide Yamaguchi,¹ Daisuke Yamauchi,³ and Shuichiro Yokoyama^{4,5}

¹*Department of Physics, Tokyo Institute of Technology,
2-12-1 Ookayama, Meguro-ku, Tokyo 152-8551, Japan*

²*Waseda Institute for Advanced Study, Waseda University,
1-6-1 Nishi-Waseda, Shinjuku, Tokyo 169-8050, Japan*

³*Faculty of Engineering, Kanagawa University, 3-27-1 Kanagawa-ku, Yokohama, Kanagawa, 221-8686, Japan*

⁴*Kobayashi Maskawa Institute, Nagoya University, Chikusa, Aichi 464-8602, Japan*

⁵*Kavli IPMU (WPI), UTIAS, The University of Tokyo, Kashiwa, Chiba 277-8583, Japan*

(Dated: August 21, 2019)

In this paper, we fully investigate cosmological scenarios in which dark matter is non-minimally coupled to an extra scalar degree of freedom. The interaction is realized by means of conformal and disformal terms in the transformed gravitational metric. Considering linear perturbation theory, we show that the growth rate of dark matter differs from the uncoupled case and that the well-known Kaiser formula undergoes modification. As a result, redshift space distortion measurements cease to be a direct probe of the linear growth rate of total matter, since the distortion factor has an extra, coupling-dependent term. We study the effect of the coupling in three cosmological models, two conformally and one disformally coupled, and forecast the constraints on the coupling, and other cosmological parameters, from future galaxy surveys.

I. INTRODUCTION

Current astrophysical and cosmological observations point to the existence of dark matter (DM) [1–6] and dark energy (DE) [7–9], the former behaving as a pressureless (cold) fluid called cold dark matter (CDM), while the latter being responsible for the universe’s current phase of accelerated expansion. However, while a lot of different models have been proposed in the literature, the fundamental nature of these components remains unknown, giving rise to one of the most pressing mysteries in present-day cosmology.

Among many dark energy models, a modification of the gravitational sector has been widely discussed. Examples of such approach include quintessence [10], K-essence [11, 12], $f(R)$ gravity [13–16], Horndeski [17–19], Gleyzes-Langlois-Piazza-Vernizzi (GLPV) [20], and Degenerate Higher-Order Scalar-Tensor (DHOST) [21] theories. The common feature of these models is the inclusion of a scalar field ϕ , which mimics the role of the cosmological constant at late times, and their theoretical predictions, as well as observational constraints in the cosmological context, have been extensively investigated (see [22, 23] for reviews).

Another crucial question is how matter (baryons and DM) is coupled to such an extra degree of freedom. A robust way to parameterize the coupling is introducing a new metric $\bar{g}_{\mu\nu}$, related to the original one, $g_{\mu\nu}$, by conformal and disformal factors, which in general depend on the scalar field and its kinetic term [24]. If both baryons and DM couple to the same $\bar{g}_{\mu\nu}$, it is known that this non-minimally coupled theory can be mapped into the minimally coupled one, resulting in a scalar-tensor theory with the minimal coupling, converted from an original one through a disformal transformation [25]. On the other hand, if baryons and DM couple to gravity with different metrics, this kind of mapping is unavailable. Non-minimal couplings to baryons are strongly constrained by local tests of gravity both at solar-system and astrophysical scales [26, 27]. Modified gravity models usually employ screening mechanisms (e.g. chameleons [28, 29] and Vainshtein [30]) in order to explain these tight constraints [31]. Hence, it is quite natural to assume that baryons are minimally coupled, reducing the need for screening mechanisms. However, the situation changes when one considers non-minimally coupled DM, and an interaction between the scalar field and the DM particle cannot be excluded a priori (see [32] for a recent review and the references therein). The modifications introduced by the non-minimal coupling manifestly affect the cosmological scenario, and the resulting evolution of large-scale structures can be used to study said coupling.

One of the most reliable large-scale structure observable is the galaxy two-point correlation function (i.e. power spectrum), which can give information about the growth of density perturbations. Since spectroscopic surveys measure the redshift of galaxies, the observed position of each galaxy is different from the actual one, due to the combined effect of the peculiar velocity and the Hubble expansion. In other words, the power spectrum in real space does not coincide with the one in redshift space. This effect is called redshift space distortion (RSD) and it allows us to extract statistical information regarding the peculiar velocities of galaxies [33].

The next generation of spectroscopic surveys, such as PFS [34], eBOSS [35], Euclid¹ [36], and WFIRST² [37], combined with future HI galaxy surveys such as the Square Kilometre Array (SKA)³ [38–40], will improve the measurements of peculiar velocities, enabling us to test various cosmological models at an extraordinary level. The recent measurements of the cosmic microwave background (CMB) by Planck satellite [9, 41] have greatly improved our knowledge regarding the universe at its early stages, and a similar gain is awaited from the forthcoming galaxy surveys, which are expected to constrain DE to an unrivaled precision.

As reviewed in section IV, it was recently shown [42] that when only DM is non-minimally coupled to the DE scalar field, the matter linear growth rate inferred by measurements of galaxies peculiar velocities is no longer defined logarithmic derivative of the linear growth function, as in the standard Λ CDM case, but rather it has an additional dependence due to the modifications to the continuity equation. Therefore, the relation between the real space and redshift space power spectra, the so-called Kaiser formula, must be modified, and the non-minimal coupling leads to a different interpretation of the growth function for matter perturbations.

In the present work, we extend the analysis done in [42], computing explicitly the difference between the effective growth rate, inferred from the peculiar velocity, and the actual one. We consider Einstein’s theory with an additional scalar degree of freedom non-minimally coupled to DM. The coupling is introduced using a new metric, consisting of a conformal part, proportional to the gravitational metric, and another term including derivatives of the scalar field, the disformal part. We study three models, parameterized by the conformal and disformal functions, solving both the background and linear equations. Additionally, we forecast the constraints to the coupling parameter from two representative future galaxy surveys, namely, Euclid and SKA. In section II we define the framework for CDM conformally/disformally coupled to a K-essence scalar field, while in section III we present the relevant background and linear perturbation equations. We also derive the evolution equations for both baryons and DM in the quasi-static limit. In section IV we review how the modifications to the DM continuity equation, due to the non-minimal coupling, motivate the definition of the effective growth rate and reformulate the Kaiser formula. Concrete cosmological examples are studied in section V choosing three different sets of conformal and disformal coupling functions. We numerically solve both the background and linear perturbation equations and study how the interaction affects the cosmic evolution. In section VI we perform a forecast analysis and predict the constraining power from future galaxy surveys, assuming SKA2-like and Euclid-like specifications, to our choices of coupling functions. Finally, in section VII we conclude and summarize our results. In Appendix A, details on conformal and disformal transformations are summarized. Scale dependence of the mass term and dispersion relation in the quasi-static limit are discussed in Appendices B and C, respectively.

II. CONFORMALLY/DISFORMALLY COUPLED DARK MATTER

In the present paper, we consider the action of Einstein’s gravity with a general scalar field ϕ and matter fields,

$$S = \int d^4x \sqrt{-g} \left[\frac{M_{\text{Pl}}^2}{2} R[g] + \mathcal{L}_\phi[g, \phi] \right] + S_m, \quad (1)$$

where M_{Pl} is the reduced Planck mass, R is the Ricci scalar defined by the metric $g_{\mu\nu}$, \mathcal{L}_ϕ is the scalar field Lagrangian, and S_m is the action for the (non-relativistic and relativistic) matter sector. We assume that the Lagrangian for baryons and radiation are defined in the usual, i.e., with these species coupled to the metric $g_{\mu\nu}$, while DM is conformally/disformally coupled to the scalar field through the metric $\bar{g}_{\mu\nu}$, such that S_m can be written as

$$S_m = \int d^4x \left[\sqrt{-g} \mathcal{L}_i[g_{\mu\nu}, \psi_i] + \sqrt{-\bar{g}} \mathcal{L}_c[\bar{g}_{\mu\nu}, \psi_c] \right], \quad (2)$$

where the index $i = \text{b, r}$ stands for baryons and radiation, respectively, whereas ψ_c denotes the dark matter field. The transformed metric is defined as

$$\bar{g}_{\mu\nu} = A(\phi, X) g_{\mu\nu} + B(\phi, X) \phi_\mu \phi_\nu, \quad (3)$$

where $\phi_\mu = \partial_\mu \phi$. The functions A and B are called conformal and disformal factors, respectively, and, in principle, both depend on the scalar field ϕ and its kinetic term $X := -(\partial\phi)^2/2$. The case in which these couplings depend

¹ <http://www.euclid-ec.org/>

² <https://wfirst.gsfc.nasa.gov/>

³ <https://www.skatelescope.org/>

only on ϕ was investigated in [43]. For the scalar field, we consider the K-essence Lagrangian $\mathcal{L}_\phi = K(\phi, X)$, which does not change a gravitational sector, i.e., ϕ does not couple directly to R , the Ricci scalar.

The variation of the action with respect to $g^{\mu\nu}$ yields the Einstein equation,

$$M_{\text{Pl}}^2 G_{\mu\nu} = T_{\mu\nu}^{(\phi)} + T_{\mu\nu}^{(m)} + T_{\mu\nu}^{(r)}, \quad (4)$$

where $T_{\mu\nu}^{(\phi)}$, $T_{\mu\nu}^{(m)} = T_{\mu\nu}^{(b)} + T_{\mu\nu}^{(c)}$, and $T_{\mu\nu}^{(r)}$ are the scalar field, total matter, and radiation energy-momentum tensors, respectively, defined as

$$T_{(\phi)}^{\mu\nu} = \frac{2}{\sqrt{-g}} \frac{\delta(\sqrt{-g}\mathcal{L}_\phi)}{\delta g_{\mu\nu}}, \quad T_{(i)}^{\mu\nu} = \frac{2}{\sqrt{-g}} \frac{\delta(\sqrt{-g}\mathcal{L}_i)}{\delta g_{\mu\nu}}, \quad T_{(c)}^{\mu\nu} = \frac{2}{\sqrt{-g}} \frac{\delta(\sqrt{-g}\mathcal{L}_c)}{\delta g_{\mu\nu}}. \quad (5)$$

Analogously, one could define $\bar{T}_{(c)}^{\mu\nu}$, the DM energy-momentum tensor in the frame in which it is minimally coupled to gravity. It can be shown that, for a homogeneous and isotropic background, if in one frame DM is a pressureless perfect fluid, it will also be in the other. This equivalence holds up to linear order (see Appendix A).

The energy-momentum tensor of the scalar field can be directly calculated from the Lagrangian, yielding

$$T_{(\phi)}^{\mu\nu} = K g^{\mu\nu} + K_X \phi^\mu \phi^\nu, \quad (6)$$

where the subscript in K_X represents the derivative with respect to the kinetic term X . The Bianchi identity immediately implies the conservation of the total energy-momentum tensor, $\nabla^\mu T_{\mu\nu} = \nabla^\mu T_{\mu\nu}^{(\phi)} + \nabla^\mu T_{\mu\nu}^{(m)} + \nabla^\mu T_{\mu\nu}^{(r)} = 0$. Indeed, since baryons and relativistic matter are minimally coupled to the metric $g_{\mu\nu}$, their conservation equations take the usual form,

$$\nabla^\mu T_{\mu\nu}^{(i)} = 0. \quad (7)$$

On the other hand, that does not hold anymore for the scalar field or DM, individually, but rather, the sum of these components is conserved:

$$\nabla^\mu T_{\mu\nu}^{(\phi)} + \nabla^\mu T_{\mu\nu}^{(c)} = 0. \quad (8)$$

In order to derive the equation of motion for ϕ , it is useful to first calculate the following quantities⁴

$$\frac{\partial}{\partial\phi}(\sqrt{-g}\mathcal{L}_c) = \frac{\delta(\sqrt{-g}\mathcal{L}_c)}{\delta g_{\mu\nu}} \frac{\delta g_{\mu\nu}}{\delta\bar{g}_{\alpha\beta}} \frac{\delta\bar{g}_{\alpha\beta}}{\delta\phi} = \sqrt{-g} Z, \quad (9)$$

$$\frac{\partial}{\partial\phi_\mu}(\sqrt{-g}\mathcal{L}_c) = \frac{\delta(\sqrt{-g}\mathcal{L}_c)}{\delta g_{\mu\nu}} \frac{\delta g_{\mu\nu}}{\delta\bar{g}_{\alpha\beta}} \frac{\delta\bar{g}_{\alpha\beta}}{\delta\phi_\mu} = \sqrt{-g} W^\mu, \quad (10)$$

where we have defined Z and W^μ as

$$Z = \frac{1}{2A} \left[A_\phi + A_X C X (A_\phi - 2B_\phi X) \right] T_{(c)} + \frac{1}{2A} \left[B_\phi + B_X C X (A_\phi - 2B_\phi X) \right] T_{(c)}^{\mu\nu} \phi_\mu \phi_\nu, \quad (11)$$

$$W^\mu = \frac{B}{A} T_{(c)}^{\mu\nu} \phi_\nu - \frac{C}{2A} (A - 2BX) \left(A_X T_{(c)} + B_X T_{(c)}^{\alpha\beta} \phi_\alpha \phi_\beta \right) \phi^\mu. \quad (12)$$

In the above equations, $T_{(c)}$ is the trace of the DM energy-momentum tensor, while the function C is defined as

$$C = \frac{1}{A - A_X X + 2B_X X^2}, \quad (13)$$

and the subscripts ϕ and X represent the derivatives with respect to the scalar field and its kinetic term, respectively. Using these results, the variation with respect to ϕ gives the equation of motion for the scalar field,

$$(K_X g^{\mu\nu} - K_{XX} \phi^\mu \phi^\nu) \phi_{\mu\nu} + K_\phi - 2K_{\phi X} X = Q, \quad (14)$$

where Q is the deviation from the minimally coupled DM,

$$Q = \nabla_\mu W^\mu - Z. \quad (15)$$

The combination of Eqs. (8), (14) and (15) leads to

$$\nabla^\mu T_{\mu\nu}^{(c)} + Q \phi_\nu = 0. \quad (16)$$

Hence, the coupling function Q determines the exchange of energy and momentum between the scalar field and the DM component.

⁴ See Appendix A for details.

III. BACKGROUND AND LINEAR PERTURBATIONS

Let us consider linear perturbations in Newtonian gauge on a spatially flat Friedmann-Lemaître-Robertson-Walker (FLRW) metric,

$$ds^2 = -[1 + 2\Phi(t, \mathbf{x})]dt^2 + a^2(t)[1 - 2\Psi(t, \mathbf{x})]d\mathbf{x}^2, \quad (17)$$

and define the energy-momentum tensor for each fluid as

$$T^{(1)0}_0 = -\rho_I(t) [1 + \delta_I(t, \mathbf{x})], \quad (18)$$

$$T^{(1)0}_i = -[\rho_I(t) + p_I(t)] \partial_i v_I(t, \mathbf{x}), \quad (19)$$

$$T^{(1)i}_j = [p_I(t) + \delta p_I(t, \mathbf{x})] \delta_j^i + [\Sigma_I(t, \mathbf{x})]^i_j, \quad \Sigma_I^i_i = 0. \quad (20)$$

Here ρ_I is the energy density, δ_I is the overdensity; p_I and δp_I are the background pressure and its perturbation, respectively; v_I is the 3-velocity potential; and $\Sigma_I^i_j = T^{(1)i}_j - \delta_j^i T^{(1)k}_k / 3$ is the traceless part of the energy-momentum tensor. Here the index $I = b, r, c, m$ represents baryon, radiation, DM, and the total matter, and $p_I = \delta p_I = \Sigma_I = 0$ for baryon and DM (i.e. CDM) as well as the total matter.

From the above definition, the overdensity and velocity potential for the total matter fluid can be respectively expressed as

$$\delta_m = \omega_c \delta_c + \omega_b \delta_b, \quad (21)$$

$$v_m = \omega_c v_c + \omega_b v_b, \quad (22)$$

where $\omega_I = \rho_I / \rho_m$ is the fractional energy density. We also split the scalar field as $\phi(t, \mathbf{x}) \rightarrow \phi(t) + \delta\phi(t, \mathbf{x})$, and introduce the convenient notation $\delta Q(t, \mathbf{x}) = Q(t, \mathbf{x}) - Q_0(t)$, where Q_0 is a background value.

A. Background equations

At background level, Einstein equations become

$$H^2 = \frac{1}{3M_{\text{Pl}}^2} (\rho_\phi + \rho_b + \rho_c + \rho_r), \quad (23)$$

$$3H^2 + 2\dot{H} = -\frac{1}{M_{\text{Pl}}^2} \left(p_\phi + \frac{1}{3} \rho_r \right), \quad (24)$$

where $H = \dot{a}/a$, and the energy density and pressure for k-essence field are respectively given by

$$\rho_\phi = \dot{\phi}^2 K_X - K, \quad (25)$$

$$p_\phi = K. \quad (26)$$

The equation of motion for ϕ , Eq. (14), yields

$$(K_X + K_{XX} \dot{\phi}^2) \ddot{\phi} + 3H \dot{\phi} K_X + K_{\phi X} \dot{\phi}^2 - K_\phi = -Q_0, \quad (27)$$

while the energy-momentum conservation for radiation, baryons and CDM leads to the background continuity equations

$$\dot{\rho}_r + 4H\rho_r = 0, \quad (28)$$

$$\dot{\rho}_b + 3H\rho_b = 0, \quad (29)$$

$$\dot{\rho}_c + 3H\rho_c = Q_0 \dot{\phi}. \quad (30)$$

The background coupling Q_0 can be directly calculated from (15), resulting in

$$Q_0 = \frac{\rho_c}{\dot{\phi}} \frac{d\Gamma}{dt}, \quad \Gamma = \ln \left[\frac{2A - A_X \dot{\phi}^2 + B_X \dot{\phi}^4}{2\sqrt{A - B\dot{\phi}^2}} \right]. \quad (31)$$

In general, the above expression for Q_0 contains $\ddot{\phi}$ such that, in order to obtain the explicit expression of Q_0 , one needs to eliminate $\ddot{\phi}$ using the equation of motion for the scalar field, solving it for Q_0 .

Using the definitions of energy density and pressure for the scalar field, Eqs. (25) and (26), respectively, the equation of motion (27) can be rewritten as

$$\dot{\rho}_\phi + 3H(1 + w_\phi)\rho_\phi = -Q_0\dot{\phi}, \quad (32)$$

which makes, according to the Eq. (30), the conservation of sum $\rho_c + \rho_\phi$ evident. The equation of state for the scalar field is defined in the usual way: $w_\phi = p_\phi/\rho_\phi$. Furthermore, the CDM energy density can be found from Eq. (30), which yields the solution

$$\rho_c \propto a^{-3} e^{\Gamma(\phi, X)}. \quad (33)$$

At the classical level, the interaction can be interpreted as a variation in the mass of the CDM particle.

B. Linear perturbations

In linear perturbation theory, the $(0, 0)$, $(0, i)$, along with the trace and traceless part of (i, j) , components of the Einstein equation in Fourier space read, respectively,

$$2M_{\text{Pl}}^2 \left[3H(H\Phi + \dot{\Psi}) + \frac{k^2}{a^2}\Psi \right] = -\delta\rho_\phi - \rho_m\delta_m - \rho_r\delta_r, \quad (34)$$

$$2M_{\text{Pl}}^2 \left[\dot{\Psi} + H\Phi \right] = K_X\dot{\phi}\delta\phi + \rho_m v_m + \frac{4}{3}\rho_r v_r, \quad (35)$$

$$2M_{\text{Pl}}^2 \left[\ddot{\Psi} + 3H\dot{\Psi} + H\dot{\Phi} + (2\dot{H} + 3H^2)\Phi + \frac{1}{3}\frac{k^2}{a^2}(\Psi - \Phi) \right] = \delta p_\phi + \delta p_r, \quad (36)$$

$$2M_{\text{Pl}}^2 \frac{k^2}{a^2}(\Psi - \Phi) = 4\rho_r\sigma_r, \quad (37)$$

where $\delta\rho_\phi$ and δp_ϕ are the scalar field energy density and pressure perturbations, respectively, while the anisotropic shear σ is defined as

$$(\rho + p)\sigma \equiv -\left(\hat{k}_i\hat{k}_j - \frac{1}{3}\delta_{ij}\right)\Sigma^i_j, \quad (38)$$

with $\hat{k}_i := k_i/k$. From the energy-momentum tensor, Eq. (6), combined with the definitions (18) and (19), we find

$$\delta\rho_\phi = -\left(K_\phi - \dot{\phi}^2 K_{\phi X}\right)\delta\phi + \left(K_X + \dot{\phi}^2 K_{XX}\right)\dot{\phi}\delta\dot{\phi} - \left(K_X + \dot{\phi}^2 K_{XX}\right)\dot{\phi}^2\Phi, \quad (39)$$

$$\delta p_\phi = K_\phi\delta\phi + \dot{\phi}K_X\left(\delta\dot{\phi} - \dot{\phi}\Phi\right). \quad (40)$$

Here, the subscripts ϕ and X in the right-hand side represent the derivatives with respect to the background values of the scalar field and its kinetic term, respectively. We can also compute the perturbed equation of motion for the scalar field,

$$-\mathcal{A}_1\frac{k^2}{a^2}\delta\phi - m_\phi^2\delta\phi + 3\mathcal{A}_1\dot{\phi}\dot{\Psi} + \mathcal{A}_2\dot{\phi}\dot{\Phi} + \mathcal{A}_3\Phi - \mathcal{A}_2\delta\ddot{\phi} + \mathcal{A}_4\delta\dot{\phi} = \delta Q, \quad (41)$$

where

$$\mathcal{A}_1 = K_X, \quad (42)$$

$$\mathcal{A}_2 = K_X + K_{XX}\dot{\phi}^2, \quad (43)$$

$$\mathcal{A}_3 = 6H\dot{\phi}K_X + \dot{\phi}^2 K_{\phi X} + 3H\dot{\phi}^3 K_{XX} + \dot{\phi}^4 K_{\phi XX} + \ddot{\phi}(2K_X + 5\dot{\phi}^2 K_{XX} + \dot{\phi}^4 K_{XXX}), \quad (44)$$

$$\mathcal{A}_4 = -3HK_X - 3H\dot{\phi}^2 K_{XX} - \ddot{\phi}(K_{XXX}\dot{\phi}^3 + 3K_{XX}\dot{\phi}) - \dot{\phi}K_{\phi X} - \dot{\phi}^3 K_{\phi XX}, \quad (45)$$

$$m_\phi^2 = -K_{\phi\phi} + 3K_{\phi X}H\dot{\phi} + K_{\phi\phi X}\dot{\phi}^2 + \ddot{\phi}(K_{\phi X} + K_{\phi XX}\dot{\phi}^2), \quad (46)$$

and the perturbation of Q is given by

$$\begin{aligned} \delta Q = & (R_1 + R_2)\dot{\phi}\dot{\delta}_c + Q_0\delta_c + R_1\dot{\phi}\frac{k^2}{a^2}v_c + R_2\frac{k^2}{a^2}\delta\phi - 3(R_1 + R_2)\dot{\phi}\dot{\Psi} - R_3\dot{\phi}\dot{\Phi} \\ & + R_4\dot{\phi}\ddot{\Phi} + R_3\delta\ddot{\phi} + R_5\delta\dot{\phi} + R_6\delta\phi, \end{aligned} \quad (47)$$

in which, for convenience, we have defined the quantities

$$R_1 = \frac{B}{A}\rho_c, \quad (48)$$

$$R_2 = -\frac{C}{2A}(A - B\dot{\phi}^2)(A_X - B_X\dot{\phi}^2)\rho_c, \quad (49)$$

$$R_3 = \rho_c\dot{\phi}\omega_X, \quad (50)$$

$$R_4 = -Q_0(\omega + \omega_X\dot{\phi}^2) - \rho_c(\omega_\phi + 3\omega_X\ddot{\phi} + \dot{\omega}_X\dot{\phi} - \zeta_X\dot{\phi}), \quad (51)$$

$$R_5 = \omega_X Q_0\dot{\phi}^2 + \rho_c(\omega_\phi + \omega_X\ddot{\phi} + \dot{\omega}_X\dot{\phi} - \zeta_X\dot{\phi}), \quad (52)$$

$$R_6 = \omega_\phi Q_0\dot{\phi} + \rho_c(\dot{\omega}_\phi - \zeta_\phi), \quad (53)$$

with

$$\omega = (R_1 + R_2)\frac{\dot{\phi}}{\rho_c}, \quad (54)$$

$$\zeta = -\frac{1}{2A}\left[A_\phi + \frac{1}{2}CA_X\dot{\phi}^2(A_\phi - B_\phi\dot{\phi}^2)\right] + \frac{\dot{\phi}^2}{2A}\left[B_\phi + \frac{1}{2}CB_X\dot{\phi}^2(A_\phi - B_\phi\dot{\phi}^2)\right]. \quad (55)$$

The energy-momentum conservation for baryonic matter yields the standard equation,

$$\dot{\delta}_b - 3\dot{\Psi} + \frac{k^2}{a^2}v_b = 0, \quad (56)$$

$$\dot{v}_b - \Phi = 0, \quad (57)$$

while CDM follows

$$\dot{\delta}_c - 3\dot{\Psi} + \frac{k^2}{a^2}v_c = \frac{\dot{\phi}}{\rho_c}(\delta Q - Q_0\delta_c) + \frac{Q_0}{\rho_c}\delta\dot{\phi}, \quad (58)$$

$$\dot{v}_c - \Phi = \frac{Q_0}{\rho_c}(\delta\phi - \dot{\phi}v_c). \quad (59)$$

For radiation, the respective equations do not change, remaining the same as in the standard Λ CDM case.

IV. EFFECTIVE GROWTH RATE AND REDSHIFT SPACE DISTORTIONS

In this section, we derive the effective growth rate of matter perturbations for the disformally coupled CDM and show that it can significantly differ from the standard definition.

A. Quasi-static approximation

Currently, data coming from galaxy surveys are restricted to scales much smaller than the cosmological horizon. Moreover, for scales well inside the sound horizon of scalar field perturbations, one can employ the quasi-static approximation [44]. Effectively, this corresponds to dropping time derivatives, with respect to space derivatives, of metric and scalar field perturbations. Furthermore, since we are interested in the effects of the DE scalar field at late-times, we neglect the contributions from relativistic matter (radiation) here and hereafter. In such an approximation, Einstein equations become constraint equations for the gravitational potentials Φ and Ψ ,

$$\frac{k^2}{a^2}\Psi = \frac{k^2}{a^2}\Phi = -\frac{1}{2M_{\text{Pl}}^2}\rho_m\delta_m, \quad (60)$$

while Eq. (27) gives a constraint for the scalar perturbation,

$$-\mathcal{A} \frac{k^2}{a^2} \delta\phi \equiv - \left(\mathcal{A}_1 \frac{k^2}{a^2} + m_\phi^2 \right) \delta\phi = \delta Q, \quad (61)$$

where δQ is given by

$$\delta Q = (R_1 + R_2) \dot{\phi} \dot{\delta}_c + Q_0 \delta_c + R_1 \dot{\phi} \frac{k^2}{a^2} v_c + R_2 \frac{k^2}{a^2} \delta\phi. \quad (62)$$

In Eq. (61) we have defined $\mathcal{A} = \mathcal{A}(t, k)$ which in general depends on the wave-number when the Compton wavelength of the scalar field is smaller than the Hubble horizon scale. When the scalar field consists of a canonical kinetic term and the scalar mass scale is irrelevant within sub-horizon scales (see Appendix B), then we have $\mathcal{A} = 1$ and recover the previous results [42]. The continuity and Euler equations for baryon are given by

$$\dot{\delta}_b + \frac{k^2}{a^2} v_b = 0, \quad (63)$$

$$\dot{v}_b - \Phi = 0, \quad (64)$$

and those for CDM are modified as follows:

$$\dot{\delta}_c + \frac{k^2}{a^2} v_c = \frac{\dot{\phi}}{\rho_c} (\delta Q - Q_0 \delta_c), \quad (65)$$

$$\dot{v}_c - \Phi = \frac{Q_0}{\rho_c} (\delta\phi - \dot{\phi} v_c). \quad (66)$$

Using $\delta\phi$ and δQ given in Eqs. (61) and (62), these become

$$(1 - \Upsilon_1) \left(\dot{\delta}_c + \frac{k^2}{a^2} v_c \right) = \Upsilon_2 (\dot{\delta}_c - \epsilon \delta_c), \quad (67)$$

$$(1 - \Upsilon_1) \frac{k^2}{a^2} (\dot{v}_c - \Phi) = \Upsilon_3 (\dot{\delta}_c - \epsilon \delta_c), \quad (68)$$

where, for convenience, we introduced the quantities

$$\Upsilon_1 = \frac{\dot{\phi}^2}{\rho_c} \frac{\mathcal{A} R_1}{\mathcal{A} + R_2}, \quad \Upsilon_2 = \frac{\dot{\phi}^2}{\rho_c} \frac{\mathcal{A} R_2}{\mathcal{A} + R_2}, \quad \Upsilon_3 = \frac{Q_0 \dot{\phi}}{\rho_c} (1 - \Upsilon_1 - \Upsilon_2) - \epsilon \Upsilon_2, \quad (69)$$

with $\epsilon = Q_0/\mathcal{A}\dot{\phi}$. In the derivation of Eq. (68) from Eq. (66), we have eliminated v_c using Eq. (67). Note that for purely conformal couplings, i.e. $A_X = B = 0$, the functions Υ_1 and Υ_2 vanish. Taking the time derivative of the continuity equations, (63) and (65), and eliminating the metric perturbations, scalar field perturbations, and velocity terms, we obtain the following second-order differential equations for baryons and CDM, respectively,

$$\ddot{\delta}_b + 2H\dot{\delta}_b - \frac{1}{2M_{\text{Pl}}^2} \rho_m \delta_m = 0, \quad (70)$$

$$(1 - \Upsilon_1 - \Upsilon_2) \ddot{\delta}_c + 2H(1 - \mathcal{E}_1) \dot{\delta}_c - \frac{1}{2M_{\text{Pl}}^2} \left[(1 - \mathcal{E}_2) \rho_c \delta_c + (1 - \Upsilon_1) \rho_b \delta_b \right] = 0, \quad (71)$$

where we have introduced two new functions of background quantities,

$$\mathcal{E}_1 = \Upsilon_1 + \frac{1}{2H} \left[\frac{1 - \Upsilon_1}{a^2} \frac{d}{dt} \left(\frac{a^2 \Upsilon_2}{1 - \Upsilon_1} \right) - \Upsilon_3 - \epsilon \Upsilon_2 \right], \quad (72)$$

$$\mathcal{E}_2 = \Upsilon_1 + \frac{2M_{\text{Pl}}^2}{\rho_c} \left[\frac{1 - \Upsilon_1}{a^2} \frac{d}{dt} \left(\frac{a^2 \epsilon \Upsilon_2}{1 - \Upsilon_1} \right) - \epsilon \Upsilon_3 \right]. \quad (73)$$

Hence, the CDM growth function experiences a different Hubble friction, H_{eff} , and feels a different gravitational pull, G_{eff} , depending on the couplings. As a result, the evolution of δ_c itself is different from the standard uncoupled case.

B. Linear growth rate

For sub-horizon scales, the system formed by the second-order differential Eqs. (70) and (71) does not depend on the wavenumber k . Therefore, one can isolate the time dependence from the k dependence of the initial conditions and express the growing solutions for the baryon and CDM density contrasts as

$$\delta_{\text{I}}(t, \mathbf{k}) = D_{\text{I}}(t)\delta_0(\mathbf{k}). \quad (74)$$

Here, $D_{\text{I}}(t)$ is the k -independent growth factor while $\delta_0(\mathbf{k})$ represents the initial density contrasts. Another quantity which is useful in describing the evolution of the perturbations is the so-called linear growth rate, defined as

$$f_{\text{I}}(t) \equiv \frac{d \ln D_{\text{I}}}{d \ln a}, \quad (75)$$

which quantifies the rate of growth in a Hubble time. The continuity equations, (63) and (65), can then be recast in terms of the respective growth factors, and the velocity potentials become

$$v_{\text{I}}(t, \mathbf{k}) = -\frac{a^2 H}{k^2} f_{\text{I}}^{\text{eff}}(t, k)\delta_{\text{I}}(t, \mathbf{k}). \quad (76)$$

For baryons, we immediately see that $f_{\text{b}} = f_{\text{b}}^{\text{eff}}$. On the other hand, Eq. (65) implies that the *effective* linear growth rate for CDM, $f_{\text{c}}^{\text{eff}}$, can deviate significantly from the standard one:

$$f_{\text{c}}^{\text{eff}} = f_{\text{c}} - \frac{\Upsilon_2}{1 - \Upsilon_1} \left(f_{\text{c}} - \frac{Q_0}{\mathcal{A}H\dot{\phi}} \right) \equiv f_{\text{c}} + \Delta f_{\text{c}}. \quad (77)$$

Furthermore, employing Eq. (22), the *effective* linear growth rate of the total matter becomes

$$f_{\text{m}}^{\text{eff}} = \frac{\omega_{\text{c}} D_{\text{c}} f_{\text{c}}^{\text{eff}} + \omega_{\text{b}} D_{\text{b}} f_{\text{b}}}{\omega_{\text{c}} D_{\text{c}} + \omega_{\text{b}} D_{\text{b}}} \equiv f_{\text{m}} + \Delta f_{\text{m}}, \quad (78)$$

$$\Delta f_{\text{m}} = \omega_{\text{c}} \frac{D_{\text{c}}}{D_{\text{m}}} \Delta f_{\text{c}} - \omega_{\text{b}} \frac{Q_0 \dot{\phi}}{H \rho_{\text{m}}} \frac{D_{\text{c}} - D_{\text{b}}}{D_{\text{m}}}, \quad (79)$$

where $D_{\text{m}} = \omega_{\text{c}} D_{\text{c}} + \omega_{\text{b}} D_{\text{b}}$ is the total matter growth function. The first term on the right-hand side of Eq. (79) comes from the definition of the CDM effective growth rate, Eq. (77), while the second is reflex of the non-minimal coupling on the actual growth rate (in the minimally coupled case, the density ratios ω_{b} and ω_{c} are constant, while the baryon and dark matter growth function are equal; naturally, that is no longer the case for when there is a non-minimal coupling). Although $f_{\text{m}}^{\text{eff}}$ is naturally given by the growth-factor-weighted average of the effective growth rates for CDM and baryons, the non-trivial terms in the CDM continuity equation and the background dynamics lead to a deviation from f_{m} , the actual growth rate.

C. Modified Kaiser formula

Spectroscopic surveys determine the distance to galaxies using their redshift. However, this measurement includes not only the Hubble flow but also a contribution from the galaxies' peculiar velocities, which will lead to errors in the determination of distances. On large scales, galaxies tend to follow the underlying matter distribution and fall into overdense regions. As a consequence, in real space, the clustering of galaxies tends to not have a preferred direction. In redshift space, however, the galaxy maps will show an anisotropy coming from the error in the determination of distances.

On linear scales, these anisotropies can be systematically taken into account. The peculiar velocity v_{g} can be related to the total matter fluid velocity v_{m} by imposing some reasonable physical condition, such as momentum-conservation law for each galaxy [43]. In the standard case, this leads to an expression for the galaxy power spectrum in redshift space, the so-called Kaiser formula [33]

$$P_{\text{g},s}(\mathbf{k}, t) = [b_{\text{g}}(t) + f_{\text{m}}(t) \mu^2]^2 P_{\text{m}}(k, t), \quad (80)$$

where b_{g} is a linear, scale-independent bias relating the tracing population of galaxies and underlying matter field distribution, μ is the cosine of the angle between the wave vector and the line of sight, and P_{m} is the matter power

spectrum in real space. According to Eq. (74), the matter power spectrum can be written in terms of the growth factor as $P_m(k, t) = D_m^2(t)P_{m,0}(k)$, where $P_{m,0}$ is the initial matter power spectrum. Eq. (80) assumes that, since galaxies move according to a common gravitational field, its velocities are not biased with respect to the matter velocity field. This formula holds not only for Λ CDM, but also for quintessence and modified gravity models with a minimal coupling.

As previously seen, when there is an interaction in the dark sector, the velocity potential, Eq. (76), is related not to the growth rate itself but to the effective growth rate. Hence, we extend Eq. (80) to a modified Kaiser formula to take into account the coupling as

$$P_{g,s}(\mathbf{k}, t) = [b_g(t) + f_m^{\text{eff}}(t, k) \mu^2]^2 P_m(k, t), \quad (81)$$

with f_m^{eff} is given in Eq. (78). For simplicity, as suggested by the Λ CDM case [45], we assume that the relation $v_g = v_m$ holds even when CDM is non-minimally coupled to the scalar field. In fact, as long as the galaxy peculiar velocity has some dependence on the dark matter velocity field (i.e. $v_g \neq v_b$), the coupling effect on RSD measurements of the growth rate will be present. The distribution of galaxies in redshift space depends on the effective growth rate and, in principle, an interaction between dark matter and the scalar field can be probed using clustering measurements.

One way to obtain the actual growth rate is to observe the time-evolution of large-scale structures using a direct probe, e.g. tomographic weak lensing. In such a case, the measurement of the gravitational potential gives clean information about the total matter density, via the Poisson equation (60). On the other hand, to probe the coupling between dark matter and the scalar field, the linear galaxy bias can be determined at each redshift by the cross-correlation between weak lensing and galaxy clustering [46] and one can then unambiguously measure the coupling using RSD measurements.

In terms of the real space and redshift space power spectra for galaxy distribution, $P_g \equiv b_g^2 P_m$ and $P_{g,s}$ respectively, the Kaiser formula, Eq. (80), reads

$$P_{g,s}(\mathbf{k}, t) = [1 + \beta(t) \mu^2]^2 P_g(k, t), \quad (82)$$

where $\beta \equiv f_m/b_g$, which encodes the corrections due to redshift space distortions, is the redshift-distortion factor. In our setting, this quantity becomes

$$\beta^{\text{eff}} = \frac{f_m^{\text{eff}}}{b_g} = \beta + \Delta\beta, \quad (83)$$

with two contributions: the usual one, due to the peculiar velocity of galaxies, and also an additional term encompassing the modifications of the CDM continuity and Euler equations due to the non-minimal coupling. For a given choice of coupling, the latter can be characterized by

$$\frac{\Delta\beta}{\beta} = \frac{\Delta f_m}{f_m}, \quad (84)$$

where Δf_m was defined in Eq. (78). For positive values of $\Delta f_m/f_m$, the difference between the real space and redshift power spectra will be further increased, while for negative values, the coupling leads to a suppression of the redshift-distortion factor.

V. CONCRETE EXAMPLES

In this section we study three cosmological models, choosing the scalar field Lagrangian, along with the conformal and disformal factors, and discuss how the strength of the coupling changes the evolution of background and perturbed quantities. To simplify the notation, throughout this section we set the reduced Planck mass, M_{Pl} , to unity.

In what follows, we consider coupled quintessence models, with the canonical scalar field Lagrangian given by

$$K(\phi, X) = X - V(\phi), \quad (85)$$

with an inverse-power-law scalar potential [47, 48],

$$V(\phi) = M^2 \phi^{-n}, \quad (86)$$

where the slope of the potential n is a positive integer and M is a constant. The potential (86) belongs to the class of freezing models [49], in which the field rolls down the potential in the past, slowing down at the onset of the cosmic

acceleration. In the uncoupled case, this model is known to give rise to tracking solutions [10, 50]: an attractor regime in which the energy density of the scalar field is subdominant, and both its equation of state and energy density parameter are approximately constant. For a wide range of initial conditions, the evolution of the scalar field will approach the previously mentioned attractor solution, with its equation of state, for the potential (86), being given by

$$w_\phi \approx \frac{nw_M - 2}{n + 2}, \quad (87)$$

where $w_M = p_M/\rho_M$ is the equation of state parameter of the dominant fluid (matter or radiation). Cosmological models that admit tracking solutions are interesting because such behavior lessens the dependence of the scalar field dynamics on the initial condition. In fact, a well-known result is that in the uncoupled case it is possible to solve the equation of motion for ϕ analytically (see, for instance, [51]).

As for the conformal and disformal factors, we consider the following one-parameter models:

Conformal model I:

$$A(\phi, X) = e^{-2\alpha\phi}, \quad B(\phi, X) = 0. \quad (88)$$

Conformal model II:

$$A(\phi, X) = e^{-\alpha\phi^2}, \quad B(\phi, X) = 0. \quad (89)$$

Disformal model III:

$$A(\phi, X) = 1, \quad B(\phi, X) = \alpha/X. \quad (90)$$

In the above expressions, α is the dimensionless coupling constant that controls the strength of the DE/CDM interaction and must be constrained by observations. For the conformal models I and II, the continuity equation in the quasi-static limit, Eq. (67) is the standard one, with no explicit dependence on the coupling, whereas for model III the background coupling Q_0 vanishes. As will be discussed in the following sections, the most important difference between model I and model II is that, even for small values of the coupling constant, the former will deviate from the tracker solution, whilst the latter still hold, by construction, the tracker properties.

In the following subsections, we present the numerical solutions for the models considered in this work. The background and linear perturbation equations for each model were implemented in the publicly available CLASS code [52]. We assume that at early times the effect of the coupling is negligible and set the initial conditions for the scalar field using the analytic expression for the tracker solution. All plots were made using the cosmological parameters presented on TABLE I. Additionally, the value of M in Eq. (86) is found using a shooting method such that we get the desired value of Ω_ϕ , the current value of the scalar field density parameter, whereas the slope parameter n is set to 0.5. The initial energy density of cold dark matter is also found by employing the shooting method.

A. Background evolution

In order to study the background evolution, it is useful to rewrite the continuity equations for CDM and the scalar field, Eqs. (30) and (32), respectively, as

$$\dot{\rho}_c + 3H(1 + w_c^{\text{eff}})\rho_c = 0, \quad (91)$$

$$\dot{\rho}_\phi + 3H(1 + w_\phi^{\text{eff}})\rho_\phi = 0, \quad (92)$$

where we have defined the expressions for the effective equation of state as

$$w_c^{\text{eff}} = -\frac{Q_0\dot{\phi}}{3H\rho_c}, \quad (93)$$

$$w_\phi^{\text{eff}} = w_\phi + \frac{Q_0\dot{\phi}}{3H\rho_\phi}. \quad (94)$$

As long as w_c^{eff} is small, much less than unity, it is expected that the evolution of the CDM energy density is not affected drastically by the interaction. Indeed, that is the case, for small values of the coupling constant, if the kinetic energy density of the scalar field is much smaller than the CDM energy density. Furthermore, when w_ϕ^{eff} is approximately constant the evolution of ϕ has a tracking behavior, even in the coupled case.

Additionally, for the scalar field Lagrangian (85), the equation of motion for ϕ at background level, Eq. (27), becomes

$$\ddot{\phi} + 3H\dot{\phi} + V_\phi = -Q_0. \quad (95)$$

1. Conformal model I

The conformal model I, characterized by the coupling functions (88), is an example of purely conformal metric transformation. This kind of interaction was first proposed in the context of coupled quintessence in [53] and has been further investigated in [54–56]. Imposing that both terms in the right hand side of Eq. (94) are constant leads to a scaling behavior and constrains the potential to be the exponential one.

According to Eq. (31), the coupling at background level is described by

$$Q_0 = -\alpha\rho_c, \quad \Gamma = -\alpha\phi, \quad (96)$$

such that, from Eq. (33), the CDM energy density evolves as

$$\rho_c \propto a^{-3} e^{-\alpha\phi}, \quad (97)$$

while the equation of motion for the scalar field, Eq. (95), gives

$$\ddot{\phi} + 3H\dot{\phi} + V_\phi = \alpha\rho_c. \quad (98)$$

When $\alpha > 0$, since ϕ is also positive, ρ_c dilutes faster than in the uncoupled case, and energy is transferred from dark matter to the scalar field, starting around the transition from radiation to matter epoch (Fig. 1a). As a result, for a given value of Ω_c today, the CDM energy density in the past will be higher in coupled models than it would be in the uncoupled case. This leads to a shift in the time of matter-radiation equality, which will take place earlier, at a higher redshift. Also, for very small values of α (e.g. $\alpha \lesssim 0.15$ in Fig. 1b) the decay of ρ_c is more important during DE epoch, whereas for slight larger values, the energy transfer is more salient during matter epoch.

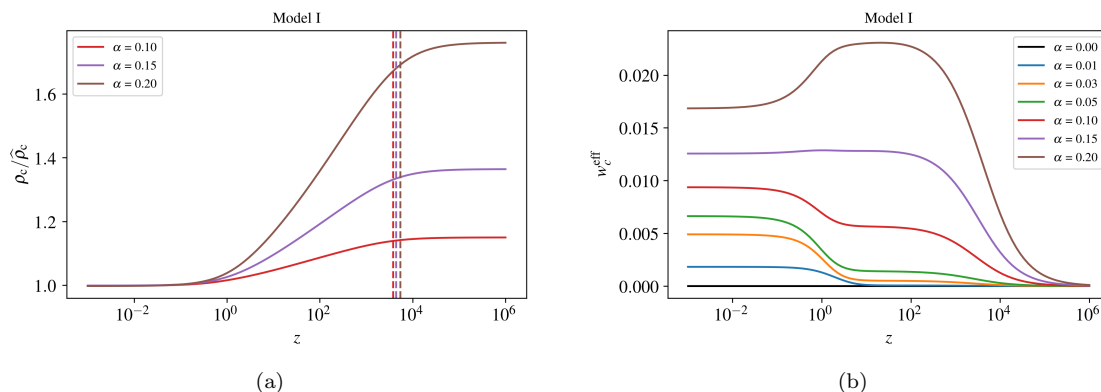


FIG. 1: Left panel (a): Evolution of the ratio between the coupled and uncoupled CDM energy density, ρ_c and $\hat{\rho}_c$, respectively. The dashed lines correspond to the redshift at matter-radiation equality. Right panel (b): Evolution of the effective equation of state of dark matter, Eq. (93). Both plots show the respective quantities as function of the redshift for the conformal model I, Eq. (88), for different values of the coupling constant.

In Fig. 2 we present the evolution of the scalar field equation of state as a function of the redshift. In the uncoupled case, ϕ follows the tracker solution with, according to Eq. (87), $w_\phi \approx -0.73$ during radiation epoch, and $w_\phi \approx -0.8$ during matter epoch. Even though the initial conditions for ϕ and $\dot{\phi}$ in the coupled case were set using the tracker solution, the evolution of the scalar field during radiation epoch is such that its kinetic energy dominates over the potential and $w_\phi \approx 1$, departing from the tracker behavior. For small values of the coupling constant (e.g. $\alpha \lesssim 0.01$), the field catches up with the tracker solution around the time of the onset of the accelerated expansion. However, for larger values of α , the evolution can deviate significantly from the uncoupled tracker solution, getting asymptotically closer to the limit $w_\phi = -1$ at the present time.

2. Conformal model II

As previously discussed, cosmological scenarios that admit scalar field tracking solutions are interesting. In the uncoupled case, the equation of state of the scalar field follows the behavior of the dominant background fluid according

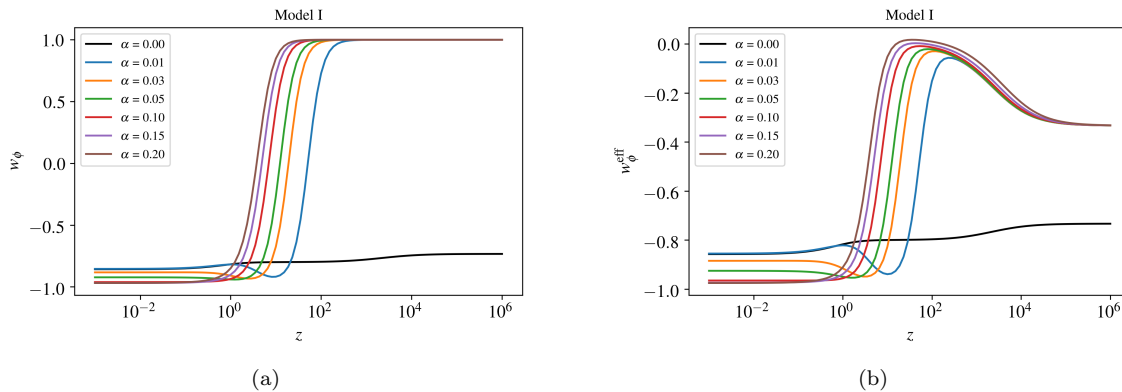


FIG. 2: Left panel (a): Evolution of the scalar field equation of state, $w_\phi = p_\phi/\rho_\phi$. Right panel (b): Evolution of the effective equation of state, Eq. (94). Both plots show the respective quantities as function of the redshift for the conformal model I, Eq. (88), for different values of the coupling constant.

to Eq. (87). Hence, during the matter-dominated epoch, for small deviation from standard uncoupled quintessence, the equation of state of the background fluid $w_m^{\text{eff}} \simeq w_c^{\text{eff}}$ would still be constant, very close to zero. Then, it is expected that Eq. (87) still holds, with $w_\phi^{\text{eff}} \simeq w_\phi$ also being approximately constant. With that in mind, by imposing a few conditions on the evolution of the scalar field, we can derive an interaction term that preserves the tracker behavior. Suppose that, during the matter domination epoch, the scalar field not only admits a tracking solution, with both terms on the right-hand side of Eq. (94) being constant, but also the ratio ρ_c/ρ_ϕ^p , for some integer $p > 1$, is constant. The exponent p guarantees that the energy density of the scalar field decreases slower than the CDM energy density, eventually becoming dominant. In such case, we have $\phi \propto \dot{\phi}^{1-p}$. Since constant w_ϕ implies that $V \propto \dot{\phi}^2$, the scalar potential must be $V \propto \phi^{2/(1-p)}$. Our parameterization corresponds to $p = 5$, namely $\rho_c \propto \rho_\phi^5$. Finally, if for simplicity we assume that the conformal function $A(\phi)$ depends only on ϕ and that the disformal one is $B = 0$, the requirement that the second term on the right-hand side of Eq. (94) is constant, leads to the following expression for the background coupling:

$$Q_0 = -\alpha\rho_c\phi, \quad \Gamma = -\frac{\alpha}{2}\phi^2. \quad (99)$$

Then, from Eq. (33), the CDM energy density evolves as,

$$\rho_c \propto a^{-3} \exp\left(-\frac{\alpha}{2}\phi^2\right), \quad (100)$$

and the equation of motion for the scalar field, Eq. (95), becomes

$$\ddot{\phi} + 3H\dot{\phi} + V_\phi = \alpha\rho_c\phi. \quad (101)$$

Similarly to model I, for positive values of the coupling constant, ρ_c dilutes faster than in the uncoupled case, and there is an injection of energy from CDM to the scalar field. However, note that the conformal factor (89) has an additional ϕ dependence on the exponential term, when compared to model I. Typically, during the cosmic evolution, the dynamics are such that $0 < \phi(t) < 1$, in reduced Planck mass units. Hence, in comparison to model I, the interaction in the dark sector for model II becomes relevant at later times, around the transition from matter to DE domination epochs, when the scalar field becomes large enough to flatten the potential (Fig. 3a). This is reflection of the fact that, by construction, model II effectively preserves the tracker properties up to the transition from matter to scalar field domination epochs. To get the same energy density at earlier times as in model I, the corresponding coupling constant must be significantly larger, and the ratio ρ_c/ρ_c increases steeply (as function of redshift) at late times. The effective equation of state for CDM remains close to zero during most part of the cosmic expansion (Fig. 3b) such that the evolution ρ_c does not deviate much from the uncouple behavior, except at the low- z region.

In this model the evolution of the coupled scalar field indeed exhibits a tracker behavior up to matter domination epoch, when the scalar field equation of state is roughly constant, Fig. 4a, but the coupling slightly changes the value of w_ϕ . However, this change is compensated by the Q_0 term in Eq. (94) such that the effective equation of state in the coupled case does not change with the interaction, remaining close to the uncoupled one, Fig. 4b. In contrast to model I, for larger values of the coupling constant, the kinetic energy of the scalar field becomes more important when compared to the scalar potential, and w_ϕ is less negative at late times.

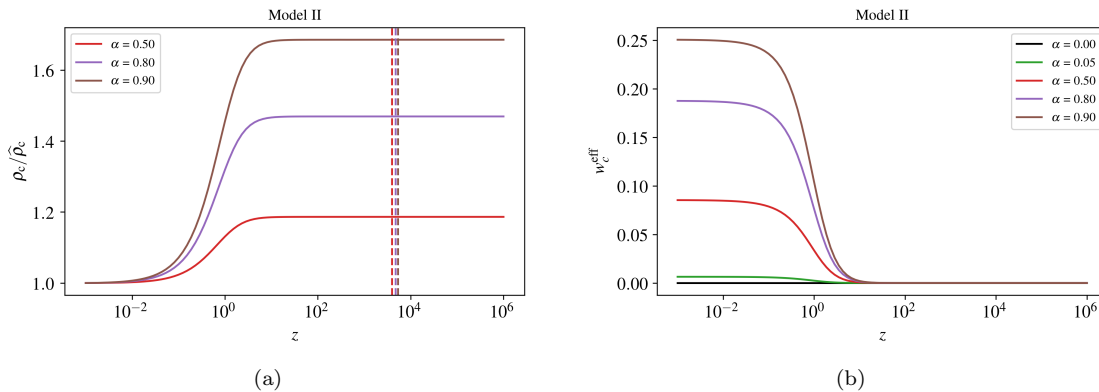


FIG. 3: Left panel (a): Evolution of the ratio between the coupled and uncoupled CDM energy density, ρ_c and $\widehat{\rho}_c$, respectively. The dashed lines correspond to the redshift at matter-radiation equality. Right panel (b): Evolution of the effective equation of state of dark matter, Eq. (93). Both plots show the respective quantities as function of the redshift for the conformal model II, Eq. (89), for different values of the coupling constant.

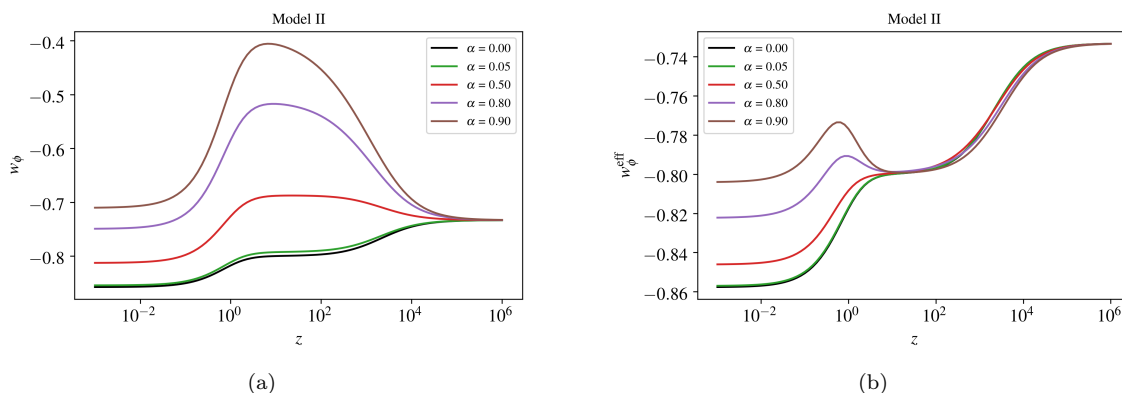


FIG. 4: Left panel (a): Evolution of the scalar field equation of state, $w_\phi = p_\phi/\rho_\phi$. Right panel (b): Evolution of the effective equation of state, Eq. (94). Both plots show the respective quantities as function of the redshift for the conformal model II, Eq. (89), for different values of the coupling constant.

3. Disformal model III

As an example of purely disformal coupling, we consider model III, characterized by the coupling functions (89). In this case, there is no interaction at the background level, $Q_0 = 0$. Hence, the energy density of cold dark matter evolves the usual way, $\rho_c \propto a^{-3}$, and the equation of motion for the scalar field is

$$\ddot{\phi} + 3H\dot{\phi} + V_\phi = 0. \quad (102)$$

From the observational point of view, the lack of modifications at background level with respect to the standard quintessence scenario is interesting, given the current constraints on the properties of the homogeneous universe. The effects induced by the DE/CDM interaction are limited to change the evolution of linear perturbations only.

B. Perturbations

In this subsection, we present the evolution of linear perturbations and study each model in the quasi-static limit. Even though all the numerical results presented in this work were computed using the full set of k -dependent linear perturbation equations shown in section III, it is elucidating to study the evolution in the quasi-static limit, since in said limit, one can write the equations of motion for the linear density in a simple way, allowing a straightforward discussion of the effects due to the coupling. Furthermore, as previously discussed, for cosmological scales probed by

galaxy surveys, said approximation is valid and there is no loss of physical information. In what follow, we present the evolution of perturbations for modes with $k = 1h \text{ Mpc}^{-1}$. We numerically checked that these modes are sufficiently deep inside the sound horizon of scalar perturbation (see Appendix C) and that the quasi-static approximation is indeed valid.

1. Conformal model I

In model I, since the coupling is purely conformal, both Υ_1 and Υ_2 , given by Eq. (69), vanish and the equation of motion for the CDM growth function, Eq. (65), becomes

$$\ddot{D}_c + 2H(1 - \mathcal{E}_1)\dot{D}_c - \frac{1}{2}[(1 - \mathcal{E}_2)\rho_c D_c + \rho_b D_b] = 0, \quad (103)$$

with the the following contributions to the Hubble friction and gravitational constant terms, respectively:

$$\mathcal{E}_1 = \frac{\alpha \dot{\phi}}{2H}, \quad \mathcal{E}_2 = -2\alpha^2. \quad (104)$$

First, by inspecting Eqs. (94) and (99), note that $\mathcal{E}_1 = 3w_c^{\text{eff}}/2$, being proportional to the square root of the fractional kinetic energy of the scalar field such that, for small values of the coupling constant α , the usual Hubble friction term is recovered at early times. On the other hand, since \mathcal{E}_2 gives a constant contribution, the conformal coupling (88) changes the gravitational constant term by a factor $\sim \mathcal{O}(\alpha^2)$ at all epochs. For $\alpha > 0$, the interaction suppresses the friction term and enhances the gravitational pull, leading to more growth (Fig. 5a). This is a general feature of models with non-minimal couplings, where the interaction between matter particles is mediated by a scalar field, leading to an attractive fifth-force. As it will be shown, this behavior is also present in models II and III.

Besides, since Υ_2 vanishes, according to Eq. (77) the effective and actual growth rates for CDM coincide. Even though $\Delta f_c = 0$, the effective linear growth rate for total matter, Eq. (78), will differ from the actual growth rate, by a factor $\sim \mathcal{O}(\alpha^2)$, due to the combined effect of the background coupling Q_0 and the difference between the baryon and CDM growth functions (Fig. 5b). Hence, the non-minimal coupling reinforces the redshift-distortion factor.

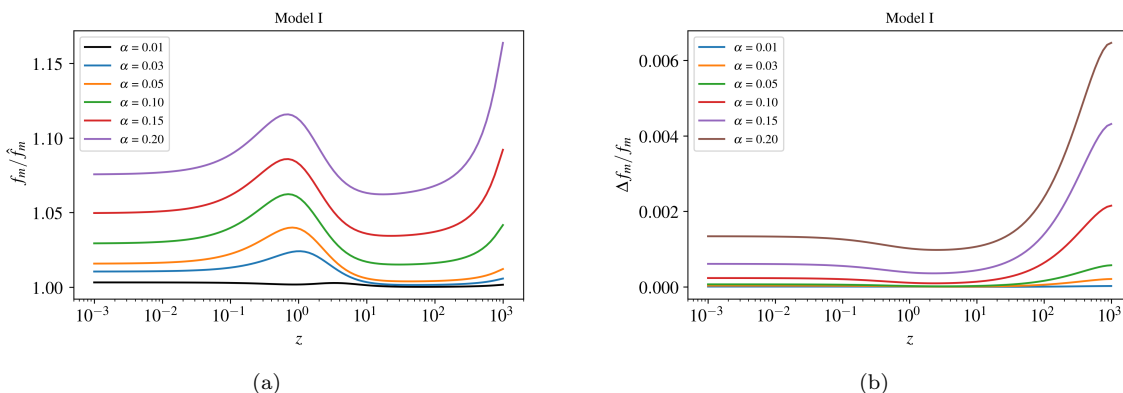


FIG. 5: Right panel (a): ratio f_m / \hat{f}_m where \hat{f}_m is the growth rate in the uncoupled case and f_m is the one with non-zero coupling. Left panel (b): difference between the effective and actual growth rates $\Delta f_m / f_m$, Eq. (78). Both figures are shown as function of the redshift for the conformal model I, Eq. (88), for different values of the coupling constant.

Let us now turn to the matter power spectrum (Fig. 6). On small scales, i.e. in the quasi-static limit, since the scalar interaction induces more growth on the CDM linear density, the power spectrum on those scales will be equally augmented. Also, since larger α makes the matter-radiation equality to take place earlier, when the Hubble horizon was smaller, the wavelength of modes that entered the horizon at the equality will be smaller. Hence, the whole power spectrum will be shifted towards larger values of k . Another effect related to the background dynamics is that, since the ratio ρ_b / ρ_m at early times decreases for larger values of the coupling constant, the amplitude of the baryon acoustic oscillations also decreases.

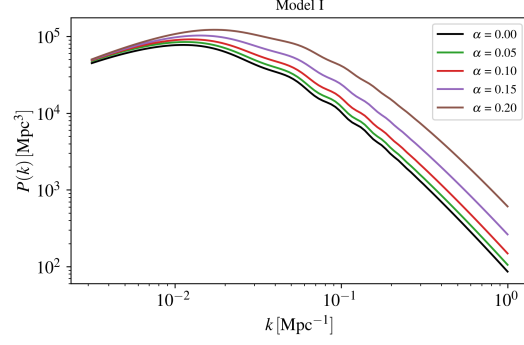


FIG. 6: Linear matter power spectrum for conformal model I, Eq. (88), for different values of the coupling constant.

2. Conformal model II

In model II, once again, both Υ_1 and Υ_2 vanish and the modifications to the evolution of dark matter growth function appear through

$$\ddot{D}_c + 2H(1 - \mathcal{E}_1)\dot{D}_c - \frac{1}{2}[(1 - \mathcal{E}_2)\rho_c D_c + \rho_b D_b] = 0, \quad (105)$$

where

$$\mathcal{E}_1 = \frac{\alpha \phi \dot{\phi}}{2H}, \quad \mathcal{E}_2 = -2\alpha^2 \phi^2. \quad (106)$$

As in conformal model I, the modification to the Hubble friction term is related to the effective CDM equation of state by $\mathcal{E}_1 = 3w_c^{\text{eff}}/2$. Once again, the correction to the Hubble friction and gravitational constant terms are $\mathcal{O}(\alpha)$ and $\mathcal{O}(\alpha^2)$, respectively, and the scalar force leads to more clustering. Similarly to the behavior at background level, since both \mathcal{E}_1 and \mathcal{E}_2 are ϕ -suppressed, the growth function during matter domination epoch does not differ significantly from the uncoupled one during matter epoch, and all the coupling-induced growth happens at late times (Fig. 7b). Hence, in order to get a deviation from the uncoupled growth function comparable to the one in model I, the value of the coupling constant must be considerably larger (Fig. 8a).

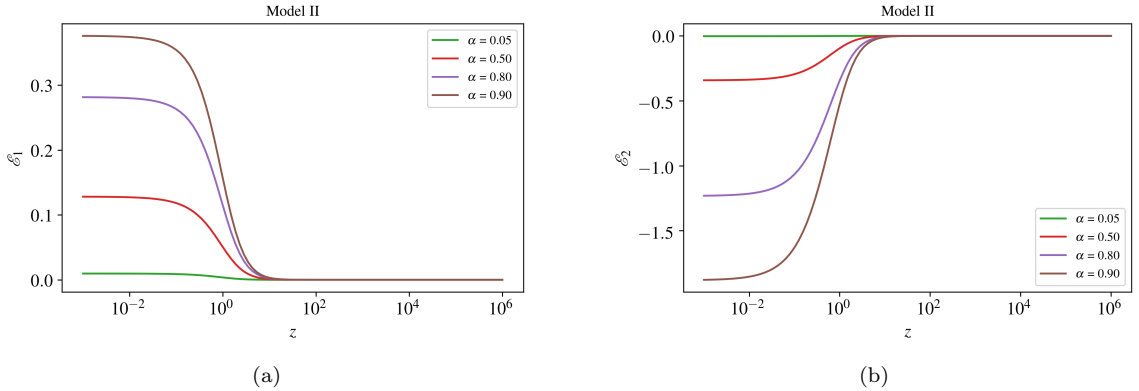


FIG. 7: Evolution of the additional Hubble friction \mathcal{E}_1 (left panel (a)) and gravitational constant \mathcal{E}_2 (right panel (b)), Eq. (106), as function of redshift for the conformal model II, Eq. (89), for different values of the coupling constant.

As in model I, Δf_c is zero and the deviation between effective and actual matter growth rate, also by a factor $\sim \mathcal{O}(\alpha^2)$, is due to the background coupling and the difference between the baryon and CDM growth function (Fig. 8b). However, since in model II the quantity \mathcal{E}_2 is negligible at early times, the difference Δf_m is present only at later epochs. Since Δf_m is positive, on top of the enhancement of the actual growth rate due to the coupling, the effective growth will be further enhanced.

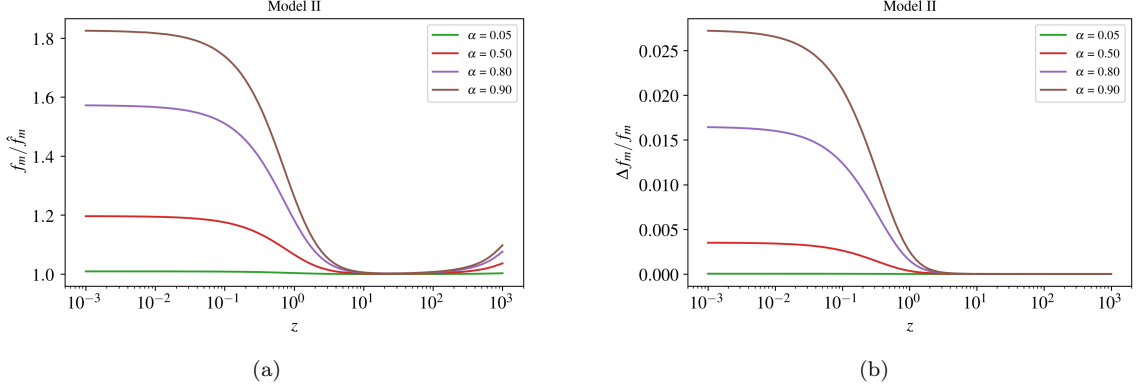


FIG. 8: Left panel (a): ratio f_m / \hat{f}_m where \hat{f}_m is the growth rate in the uncoupled, case and f_m is the one with non-zero coupling. Right panel (b): difference between the effective and actual growth rates $\Delta f_m / f_m$, Eq. (78). Both figures are shown as function of the redshift for the conformal model II, Eq. (89), for different values of the coupling constant.

The behavior of the matter power spectrum of linear perturbations in model II (Fig. 9) resembles that of model I. For larger values of the coupling constant, because of the clustering induced by the coupling, it is enhanced at small scales, whereas the change in the time of matter-radiation equality shifts the whole spectrum towards larger values of k . The amplitude of the baryonic feature also decreases. However, since the interaction is effective only during the scalar-field-dominated epoch, to get a modification of the same effect as in model I, the coupling constant must be roughly one order of magnitude larger.

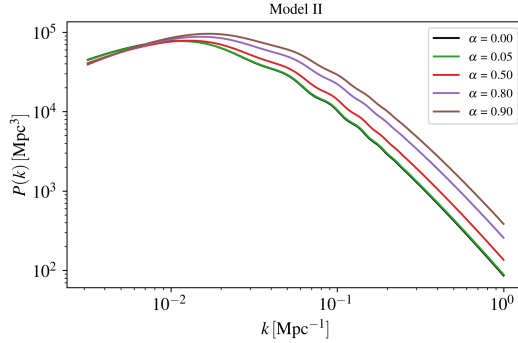


FIG. 9: Linear matter power spectrum for conformal model II, Eq. (89), for different values of the coupling constant.

3. Disformal model III

For model III, with conformal and disformal factors defined in Eq. (90), one finds $\Upsilon_1 = -\Upsilon_2 = \mathcal{E}_2$. Hence, the equation of motion for the CDM growth function, Eq. (65), becomes

$$\ddot{D}_c + 2H(1 - \mathcal{E}_1)\dot{D}_c - \frac{1}{2}(1 - \mathcal{E}_2)(\rho_c D_c + \rho_b D_b) = 0, \quad (107)$$

where,

$$\mathcal{E}_1 = -\frac{2\alpha^2 \rho_c \dot{\phi} (3H\dot{\phi} + 2V_\phi)}{H(\dot{\phi}^2 - 2\alpha\rho_c) \left[(1 - 2\alpha)\dot{\phi}^2 - 2\alpha\rho_c \right]}, \quad \mathcal{E}_2 = \frac{2\alpha\dot{\phi}^2}{\dot{\phi}^2 - 2\alpha\rho_c}. \quad (108)$$

Note that, in principle, when $\dot{\phi}^2 = 2\alpha\rho_c$ both \mathcal{E}_1 and \mathcal{E}_2 functions diverge, whereas when $(1 - 2\alpha)\dot{\phi}^2 - 2\alpha\rho_c = 0$ only \mathcal{E}_1 has problems. The requirement that the disformally transformed metric $\bar{g}_{\mu\nu}$ preserves the Lorentzian signature for

this choice of the functions A and B translates into $2\alpha < 1$ (see Appendix A), which by itself does not guarantee that the functions \mathcal{E}_1 and \mathcal{E}_2 are well defined. However, the disformal coupling modifies the sound speed of the scalar field, not being equal to unity as it is the case for standard quintessence. The requirement that $c_s^2 > 0$ leads to the constraint $\alpha < \dot{\phi}^2/(2\rho_c)$, the ratio between the scalar field kinetic energy and the CDM energy density (see Appendix C). Since this relation must be satisfied throughout the cosmic evolution, we consider only negative values for the coupling constant. Similarly to model II, at earlier times the functions \mathcal{E}_1 and \mathcal{E}_2 are negligibly small, so the growth rate is insensitive to the interaction, and most of the effects due to the coupling become important during onset of the DE scalar field domination epoch (Fig. 10). That is a consequence of the fact that both functions depend not only on the coupling constant, but also on the ratio between the kinetic energy of the scalar field, $\dot{\phi}^2/2$, and the CDM energy density. During matter domination epoch, this ratio is negligibly small, such that both \mathcal{E}_1 and \mathcal{E}_2 remain close to zero, regardless of the coupling constant value. However, as the ratio gets closer to unity at late times, the coupling becomes significant, with \mathcal{E}_1 and \mathcal{E}_2 being roughly proportional to α^2 and α , respectively.

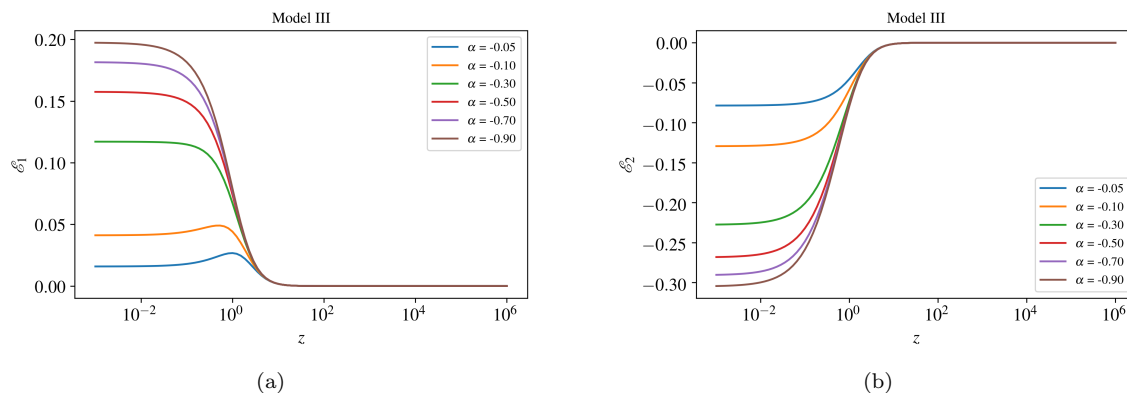


FIG. 10: Evolution of the additional Hubble friction \mathcal{E}_1 (left panel (a)) and gravitational constant \mathcal{E}_2 (right panel (b)), Eq. (108), as function of redshift for the disformal model III, Eq. (90), for different values of the coupling constant.

Naturally, this choice of disformal factor also leads to more growth, since the Hubble friction is suppressed, while the gravitational constant term is enhanced (Fig. 11a). However, in contrast with the conformal models I and II, increasing the value of $|\alpha|$ indefinitely does not lead to more growth. Indeed, taking the limit $\alpha \rightarrow -\infty$, one finds

$$\mathcal{E}_1 \rightarrow -\frac{\dot{\phi} (3H\dot{\phi} + 2V_\phi)}{2H(\dot{\phi}^2 + \rho_c)}, \quad \mathcal{E}_2 \rightarrow -\frac{\dot{\phi}^2}{\rho_c}, \quad (109)$$

which means that the modifications due to the coupling saturate.

The lack of modification at the background level implies that the deviation of f_m^{eff} from f_m is due only to the term proportional to Δf_c in equation (78). At late times, when $\dot{\phi}^2/(2\rho_c) \sim 1$, it becomes $\Delta f_c \approx 2\alpha f_c/(1-3\alpha)$. In contrast to the conformally coupled models, Δf_m for model III is negative (Fig. 11b), being roughly proportional to α for small values of the coupling constant. Therefore, the enhancement of the actual growth rate due to the coupling will be suppressed. However, as in the case of the growth function, $|\Delta f_m|$ does not increase indefinitely when one consider larger and larger values of $|\alpha|$.

Once again, because of the lack of modifications at the background level, the amplitude of the power spectrum simply increases, due to the coupling effect on the growth function, as shown in Fig. 12.

VI. FORECASTS

In this section, we introduce the approach followed to obtain the constraining power of future galaxy surveys on cosmological parameters.

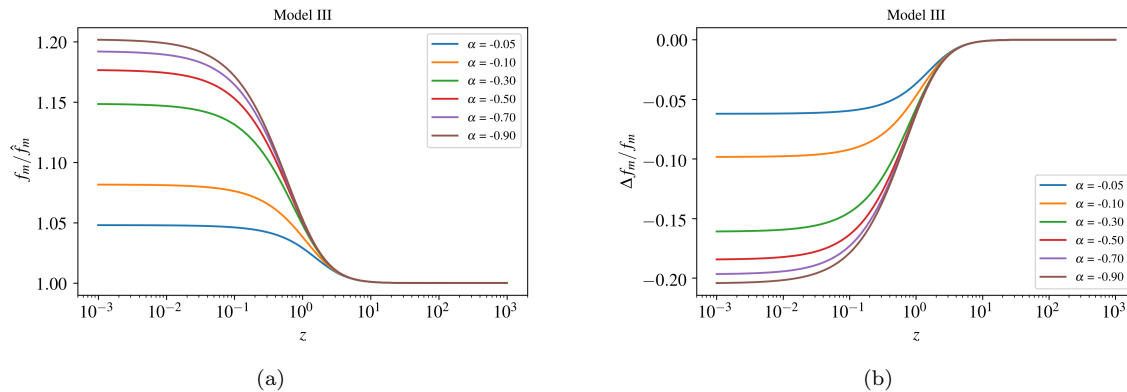


FIG. 11: Left panel (a): ratio f_m / \hat{f}_m where \hat{f}_m is the growth rate in the uncoupled, case and f_m is the one with non-zero coupling. Right panel (b): difference between the effective and actual growth rates $\Delta f_m / f_m$, Eq. (78). Both figures are shown as function of the redshift for the disformal model III, Eq. (90), for different values of the coupling constant.

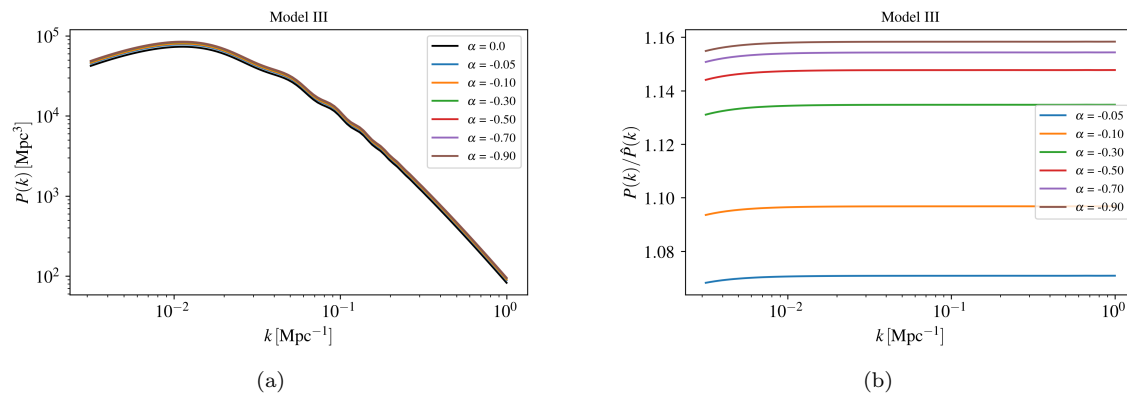


FIG. 12: Left panel (a): linear matter power spectrum. Right panel (b): ratio $P(k) / \hat{P}(k)$ where $\hat{P}(k)$ is the power spectrum in the uncoupled case, and $P(k)$ is the one with non-zero coupling. Both spectra are computed at the redshift $z = 0$ for the disformal model III, Eq. (90), for different values of the coupling constant.

A. Method

In order to forecast how well the future galaxy surveys will be able to constraint the DE/CDM coupling, we employ the Fisher matrix analysis to the galaxy power spectrum sliced over several redshift bins. The technique consists of approximating the full likelihood for the cosmological parameters as a multivariate Gaussian distribution. After Taylor expanding the likelihood function \mathcal{L} , the Fisher matrix is defined by

$$F_{\alpha\beta} = - \left\langle \frac{\partial^2 \ln \mathcal{L}(\theta)}{\partial \theta^\alpha \partial \theta^\beta} \right\rangle \Big|_{\hat{\theta}}, \quad (110)$$

where $\hat{\theta}$ is the vector containing the maximum likelihood estimators. The Fisher matrix estimates the best possible precision obtainable by a given experiment. Under the assumption that the parameters follow a Gaussian distribution, the Fisher matrix is the inverse of the covariance matrix. Generally, that is the case near the peak of the likelihood, and the Fisher matrix provides a good approximation to the uncertainties. The marginalized constraint on a given parameter θ^α is simply $(F^{-1})_{\alpha\alpha}^{1/2}$, while the unmarginalized one, when all the other parameters are fixed, is given by $(F_{\alpha\alpha})^{-1/2}$. As long as the parameters are not extremely degenerated, the Fisher matrix method is an efficient tool in estimating the best possible constraints.

When applied to galaxy power spectrum observations, sliced over several redshift bins, the Fisher matrix takes the

form [57, 58],

$$F_{\alpha\beta} = \sum_{z_i} \int_{k_{\min}}^{k_{\max}} \frac{d^3 \mathbf{k}}{(2\pi)^3} V_{\text{eff}}(\mathbf{k}, z_i) \frac{\partial \ln P_{\text{obs}}(\mathbf{k}, z_i)}{\partial \theta^\alpha} \frac{\partial \ln P_{\text{obs}}(\mathbf{k}, z_i)}{\partial \theta^\beta}, \quad (111)$$

where the effective volume V_{eff} is defined as

$$V_{\text{eff}}(\mathbf{k}, z_i) = \left(\frac{n_g(z_i) P_{\text{obs}}(\mathbf{k}, z_i)}{n_g(z_i) P_{\text{obs}}(\mathbf{k}, z_i) + 1} \right)^2 V_{\text{survey}}(z_i), \quad (112)$$

which comes from the fact that, since galaxies follow a Poissonian distribution, the observed power spectrum has a shot-noise correction $P_{\text{shot}} = n_g^{-1}$, with $n_g(z_i)$ being the number density of galaxies in a redshift bin. When the sampling is good enough, $n_g P_{\text{obs}} \gg 1$ and both effective and actual survey volumes coincide. Note that the total Fisher matrix is given by the summation over all redshift bins of the integrals over \mathbf{k} .

To compute the observed galaxy power spectrum, in addition to the modified Kaiser effect discussed in section (IV C), a few other effects must be taken into account, and the general expression reads [58]

$$P_{\text{obs}}(\mathbf{k}, z) = \mathcal{N}_{\text{AP}}(z) [b_g(z) + f_m^{\text{eff}}(z)\mu^2]^2 P_m(k, z) e^{-k^2 \mu^2 \sigma_{\text{NL}}^2}. \quad (113)$$

The Alcock-Packzyski factor [59], defined as

$$\mathcal{N}_{\text{AP}}(z) = \left(\frac{D_A^{\text{ref}}(z)}{D_A(z)} \right)^2 \frac{H(z)}{H^{\text{ref}}(z)}, \quad (114)$$

where D_A is the angular diameter distance and H is the Hubble function, is a correction due to the fact that when converting angles and redshifts into distances and wavenumbers one needs to, incorrectly, assume a reference cosmology. On the other hand, the exponential factor corresponds to errors in the observed redshift due to a line-of-sight smearing of the structure [60], which becomes relevant on small scales, and is characterized by the nuisance parameter σ_{NL} . Finally, we can compute the derivative of the observed galaxy power spectrum with respect to the cosmological parameters, resulting in [60]

$$\begin{aligned} \frac{d \ln P_{\text{obs}}}{d\theta^\alpha} &= \frac{\partial \ln P_m}{\partial \theta^\alpha} + \frac{2}{b_g + f_m^{\text{eff}} \mu^2} \left(\frac{\partial b_g}{\partial \theta^\alpha} + \mu^2 \frac{\partial f_m^{\text{eff}}}{\partial \theta^\alpha} \right) - k^2 \mu^2 \frac{\partial \sigma_{\text{NL}}^2}{\partial \theta^\alpha} \\ &+ \left[1 + \frac{4 f_m^{\text{eff}} \mu^2}{b_g + f_m^{\text{eff}} \mu^2} (1 - \mu^2) + \frac{\partial \ln P_m}{\partial \ln k} \mu^2 - 2 k^2 \mu^2 \sigma_{\text{NL}}^2 \right] \frac{d \ln H}{d\theta^\alpha} \\ &+ \left[-2 + \frac{4 f_m^{\text{eff}} \mu^2}{b_g + f_m^{\text{eff}} \mu^2} (1 - \mu^2) - \frac{\partial \ln P_m}{\partial \ln k} (1 - \mu^2) \right] \frac{d \ln D_A}{d\theta^\alpha}. \end{aligned} \quad (115)$$

In this work, we perform the forecast for the set of cosmological parameters

$$\boldsymbol{\theta} = \{\alpha, h, \Omega_b h^2, \Omega_\phi, 10^9 A_s, n_s\} + \{\sigma_{\text{NL}}, b_g(z_i)\}, \quad (116)$$

where α is the coupling constant for each model considered here, h is the dimensionless Hubble parameter, defined as $H_0 = 100h \text{ km/s/Mpc}$, Ω_b and Ω_ϕ are, respectively, the baryon and scalar field current density parameters, A_s is the amplitude of the primordial power spectrum at $k = 0.05 \text{ Mpc}^{-1}$, and n_s is the spectral index of primordial perturbations. The error in the observed redshift, σ_{NL} , and the galaxy bias at each redshift bin, $b(z_i)$, are taken to be nuisance parameters and are marginalized over. Further, we consider a flat geometry.

For each model, the fiducial values for the coupling constant is chosen to be

- Conformal model I: $\alpha = 0.05$.
- Conformal model II: $\alpha = 0.1$.
- Disformal model III: $\alpha = -0.05$.

This choice for the conformal model I is consistent with current constraints on coupled quintessence [61]. Even though we are interested in cosmological scenarios that differ from the standard one, we set the fiducial cosmology using current constraints on ΛCDM [41]. These values are shown in TABLE I. We choose the value $\sigma_{\text{NL}} = 7 \text{ Mpc}$, corresponding to a peculiar velocity dispersion of roughly 400 km/s [62, 63]. Moreover, we assume that the slope

TABLE I: Fiducial cosmological parameters consistent with Planck 2018 results for Λ CDM [41]

Parameter	h	$\Omega_b h^2$	Ω_ϕ	$10^9 A_s$	n_s
Value	0.674	0.224	0.685	2.10	0.965

of the scalar field potential n is fixed, and set its value to $n = 0.5$, which is consistent with current constraints on quintessence [61].

Our goal is estimating the precision with which future galaxy redshift surveys will be able to measure the set of cosmological parameters (116), especially the coupling constant α .

In this work, we consider experiments with Euclid-like [64] and SKA-like (Phase 2) [65] configurations. For the Euclid-like survey, we consider the range $0.7 < z < 2$, with a sky coverage of 15,000 squared degrees, and bias function $b_g = \sqrt{1+z}$, while for SKA2 we take $0.1 < z < 2$, a sky coverage of 30,000 squared degrees, and bias function $b_g = c_1 \exp(c_2 z)$, with constants c_1 and c_2 given in [65]. We adopt the predicted number density of galaxies as a function of redshift given in [64] and [65]. We divide the survey volume into redshift bins, with $\Delta z = 0.1$, and consider the expect galaxy number density $n_g(z_i)$ and galaxy bias $b_g(z_i)$ at each redshift slice z_i .

At each redshift bin, the limits of integration in Eq. (111) are taken to be

$$k_{\min}(z_i) = \left(\frac{2\pi}{V_{\text{survey}}(z_i)} \right)^{1/3}, \quad k_{\max}(z_i) = 0.2h(1+z_i)^{2/(2+n_s)}, \quad (117)$$

for both surveys. The maximum wavenumber k_{\max} corresponds to a conservative cut-off of non-linear scales [66, 67].

The derivative with respect to a given cosmological parameter θ^α in the Fisher matrix are performed numerically, with a symmetric difference quotient, evaluating the observed power spectrum at $\theta^\alpha(1 \pm 10^{-2})$.

B. Forecast results

On TABLE II we present the marginalized 1σ C.L. errors on the fiducial parameters for all three models, while the two-dimensional contour plots for models I, II and III are presented in Figs. 13, 14 and 15, respectively. Note that, even though we did not include any prior to the value of α for the disformal model III, it must be kept in mind that the condition $\alpha < \dot{\phi}^2/(2\rho_c)$, discussed in section VB3, must be satisfied. For each fiducial model, the forecasts for SKA and Euclid are combined, marginalizing over the biases and summing the resulting Fisher matrices.

TABLE II: Results for the Fisher analysis

Model	Survey	$10^2 \times \sigma(h)$	$10^3 \times \sigma(\Omega_b h^2)$	$10^3 \times \sigma(\Omega_\phi)$	$10^2 \times \sigma(\alpha)$	$10^2 \times \sigma(10^9 A_s)$	$10^3 \times \sigma(n_s)$
I	Euclid	1.46	1.36	2.38	0.50	8.86	1.08
	SKA2	0.60	0.57	1.18	0.26	4.14	0.53
	Combined	0.55	0.52	1.06	0.22	3.61	0.46
II	Euclid	0.84	0.88	9.30	10.46	4.79	0.65
	SKA2	0.53	0.57	5.35	5.62	2.88	0.45
	Combined	0.44	0.47	4.43	4.69	2.40	0.36
III	Euclid	0.78	0.85	2.41	24.93	3.83	0.72
	SKA2	0.47	0.50	1.24	6.99	2.59	0.41
	Combined	0.40	0.42	1.07	6.23	2.13	0.35

Note that the forecasted constraints from the SKA-like survey are more stringent than those from Euclid-like one. The main driver of this result is the fact that the redshift window of SKA2 is larger than Euclid's, the former being able to measure galaxies at lower redshifts, and we assumed the same spacing for the redshift bins. Hence, the predicted errors measured by SKA are expected to be smaller.

Generally speaking, the effects of the non-minimal coupling on the observed power spectrum occur on the redshift-distortion factor, growth function, and the power spectrum (baryonic wiggles' position and shape). In the previous sections, it was shown that in model I the interaction changes the evolution of both background and linear perturbations at all epochs, while in model II the modification arises only at late times. On the other hand, in model III, the coupling does not affect the background evolution but changes the behavior of linear perturbations at late times.

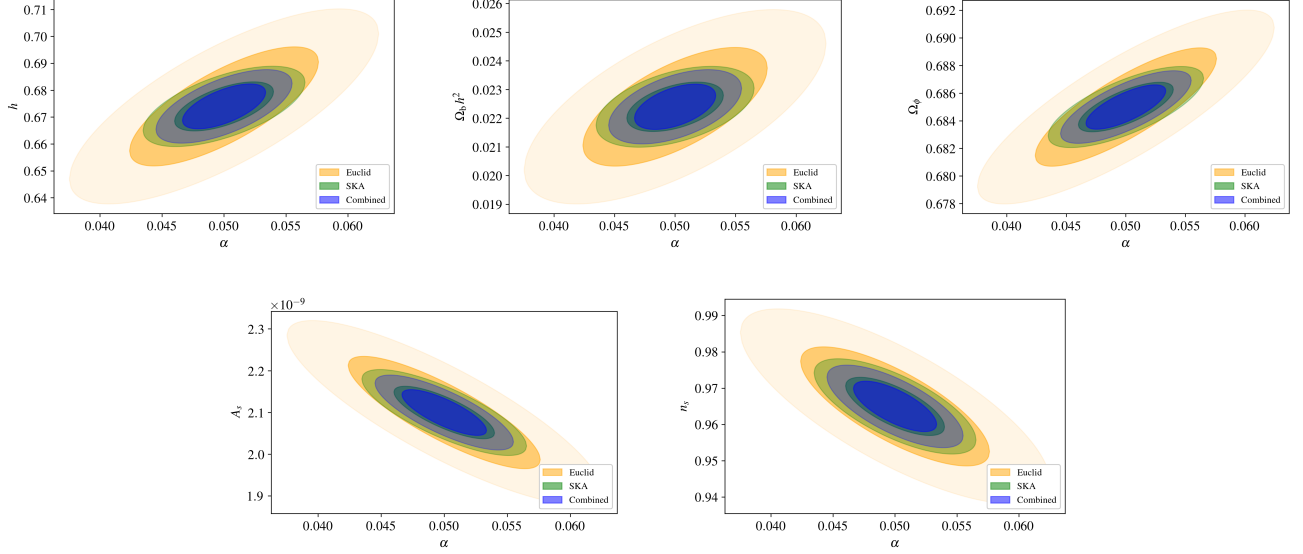


FIG. 13: Confidence regions, 1σ and 2σ , for selected parameters vs α for the conformal model I. We present the independent SKA and Euclid results, and also the combined one. The contours are obtained marginalizing over all the parameters except the ones being plotted.

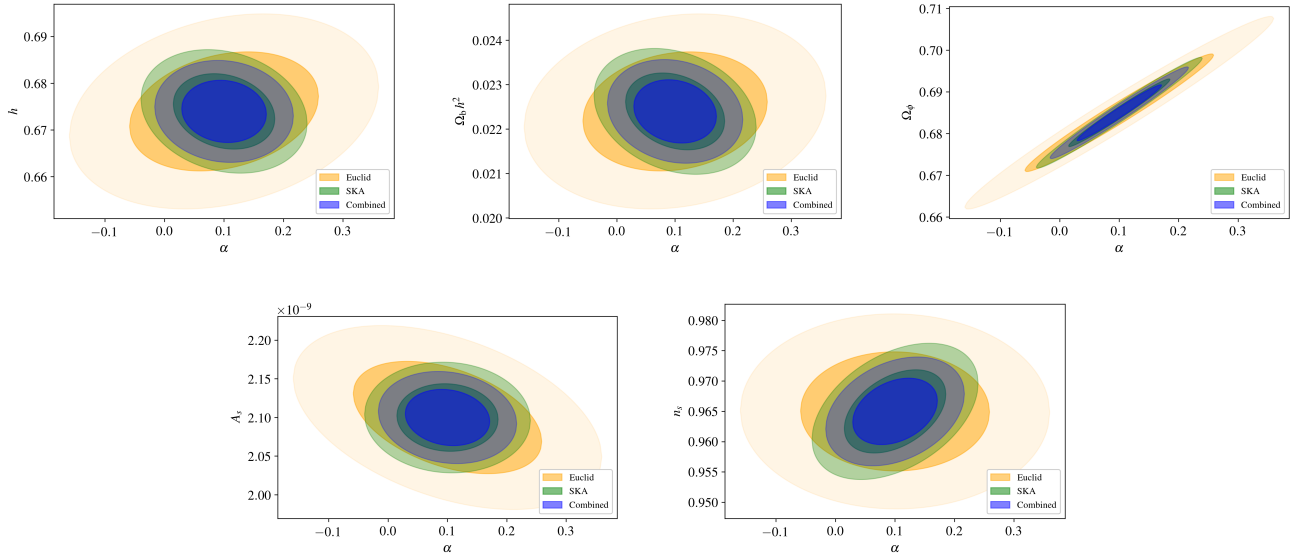


FIG. 14: Confidence regions, 1σ and 2σ , for selected parameters vs α for the conformal model II assuming a fiducial coupling constant $\alpha = 0.1$. We present the independent SKA and Euclid results, and also the combined one. The contours are obtained marginalizing over all the parameters except the ones being plotted.

Since, at the background level, the main effect of the interaction is the energy transfer from CDM to the DE scalar field, the coupling causes a degeneracy between α and Ω_ϕ . Despite the degeneracy, both surveys would be able to constraint α and Ω_ϕ for model I better than for models II and III. The reason is that in model II, the coupling affects the evolution of background and perturbed quantities only at late times, effectively being less important than in model I. In model III the coupling only changes the growth function at late times, and also, since for a given α the negative Δf_m compensates the growth, the redshift-distortion factor β is not as sensitive to the non-minimal coupling as the conformal models. However, the precision with which all the other parameters could be measured by both surveys is higher for models II and III, since in model I the modification at higher redshift leads to indetermination

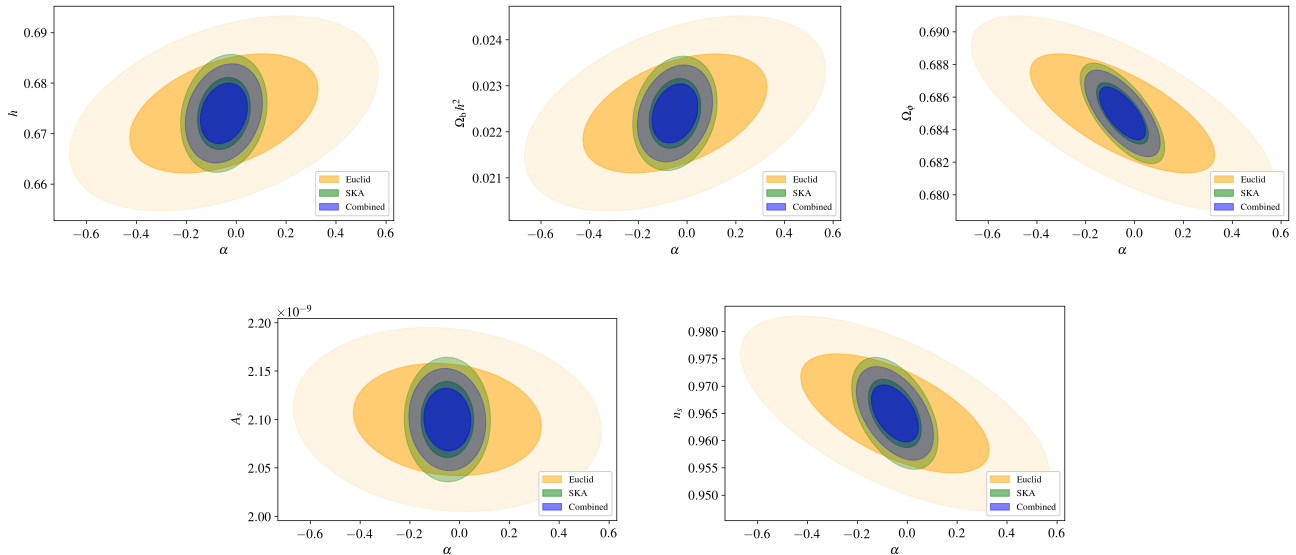


FIG. 15: Confidence regions, 1σ and 2σ , for selected parameters vs α for the disformal model III. We present the independent SKA and Euclid results, and also the combined one. The contours are obtained marginalizing over all the parameters except the ones being plotted.

on these parameters.

The constraints on all parameters except α and Ω_ϕ from SKA and Euclid are roughly of the same order of magnitude for all fiducial cosmologies considered here. In particular, for models II and III, the constraints from SKA and Euclid are of the same order of magnitude for all parameters except the coupling constant. The constraints from Euclid are much less stringent, since the modifications due to the coupling take place at low redshifts, outside its observational window. Note also that the error on Ω_ϕ for model III is comparable to the result for model I - even though the impact of the interaction is more important in the latter, the degeneracy between Ω_ϕ and α hinders the determination of Ω_ϕ .

The combined analysis helps in reducing the degeneracy and gives slightly better constraints. For all the fiducial cosmologies, the two-dimensional contour plots for (α, h) and $(\alpha, \Omega_b h^2)$ have roughly the same shape. For models II and III, since the modifications due to the non-minimal coupling are delayed in comparison to model I, these parameters show little to no correlation.

From the Fisher matrix analysis, we see that experiments with specifications similar to both surveys could determine if there is a non-minimal coupling in the dark sector for the conformal model I with our choice of fiducial cosmology. The coupling constant could be determined to the percentage level, significantly improving the current constraints [61]. For model II, the interaction could be probed to the 1σ level. On the other hand, for model III, the forecasted surveys do not have enough precision to determine the existence of the interaction, rendering these models observationally equivalent to the standard quintessence scenario. However, the combination of other cosmological probes, such as weak lensing, could help in breaking the degeneracy.

VII. CONCLUSION

In this paper, we extended the treatment of Einstein's gravity with a non-minimally coupled DM component recently presented in [42], generalizing it from the canonical scalar field Lagrangian to the general K-essence one. In our setup, the coupling between scalar field and DM is designed through the effective metric with conformal and disformal factors, whereas, to evade solar system constraints, baryon and radiation couple minimally to metric. Effectively, such dependence leads to an energy transfer between DM and DE.

At the homogeneous level, the interaction can be understood as if the mass of the DM particle depends on the value of the scalar field. As for linear perturbations, the interaction mediated by a scalar field through disformal and conformal transformations changes both the perturbed continuity and Euler equations for CDM, while baryons and radiation follow the standard equations. We showed that the modification is important even at sub-horizon scales (in the quasi-static limit) and the overall effect can be understood in terms of an effective Hubble friction and effective gravitational coupling. As a result, the growth of perturbation differs from the standard uncoupled case, and the

difference can be, in principle, observationally tested.

In the presence of an interaction, since the modified Kaiser formula provides information only about the effective linear growth rate, determined using the galaxy peculiar velocity field, single-redshift RSD measurements are not able to measure the actual growth. However, multiple-redshift RSD measurements, or a combination of different types of observations, can help in breaking the degeneracy. Therefore, when considering extensions of the Λ CDM paradigm, one must carefully take such effects into account. These statements are true not only for our setup but also for any cosmological model including DM interacting with DE, as long as the continuity equation for the total matter is modified.

In this paper, by considering three concrete cosmological models (two with purely conformal couplings and one with a disformal coupling), we studied the cosmological evolution of both background quantities and linear perturbations. The well-known coupled quintessence model, here denoted by conformal model I, does not admit a tracker solution, and the presence of the coupling changes the evolution of matter linear density even at early times due to the modification of the effective gravitational coupling. Then, we proposed an improved model, denoted by conformal model II, in which the tracker behavior is preserved even in the coupled case, and the effects of the coupling on the evolution of matter linear density become important only at late times. For both conformal models I and II, the continuity equation for CDM follows the standard one, and thus the coupling effect in the effective linear growth rate is roughly the square of the coupling constant α . We also proposed a purely disformal coupled model denoted by model III. Thanks to a particular choice of the form of the disformal factor in this model, the energy transfer at the background level does not occur, therefore the background cosmological evolution is identical to the one in quintessence model. Furthermore, an additional contribution due to the coupling in the effective gravitational constant is suppressed at early times, and the coupling effect on the effective linear growth rate, due to the modification of the continuity equation for CDM, is roughly of the same order as the coupling constant α . In all three models explored, the DE-DM coupling leads to more clustering, because of the attractive nature of the scalar fifth-force. Considering the conformal models I and II, the difference between the effective and actual linear growth rates are positive, such that RSD measurements would indicate a higher growth rate than the true one. On the other hand, for the disformal model III, the effective linear growth rate is smaller than the actual one, suppressing the redshift-distortion effect. Hence, RSD measurements have less constraining power regarding the parameters of model III when compared to models I and II.

As for the prospect of future probes measuring the DE-DM coupling, by employing the Fisher matrix analysis, we showed that assuming either of the conformal models, the absence of coupling could be probed within 1σ , with the coupling constant being measured with a percent-level precision. On the other hand, for the disformal model III, RSD measurements alone would not be able to determine the coupling constant with sufficient accuracy. It is expected that a combination of RSD, weak lensing, and CMB measurements would give better constraints on the coupling constant, and we hope to come back to this issue in the future.

Acknowledgments

We thank Teruaki Suyama for many useful comments and discussions. This work was supported in part by JSPS Grant-in-Aid for Scientific Research Nos. 17K14276 (R.K.), 18K18764 (M.Y.), 17K14304, and 19H01891 (D.Y.), MEXT KAKENHI Grant-in-Aid for Scientific Research on Innovative Areas Nos. 15H05888, 18H04579 (M.Y.), and 18H04356 (S.Y.). This work was also partially supported by the Mitsubishi Foundation (M.Y.), JSPS and NRF under the Japan-Korea Basic Scientific Cooperation Program (M.Y. and S.Y.), and JSPS Bilateral Open Partnership Joint Research Projects (F.C., R.K., and, M.Y.).

Appendix A: Metric transformation

In this appendix, we summarize the expressions needed in deriving the equations of motion.

The disformal metric transformation [24] is defined as

$$\bar{g}_{\mu\nu} = A(\phi, X)g_{\mu\nu} + B(\phi, X)\phi_\mu\phi_\nu, \quad (\text{A1})$$

where A and B are called, respectively, conformal and disformal functions. In order to have a well-behaved 'new' metric, the transformation must preserve the Lorentzian signature and the causal structure (since the disformal factor changes the light-cones), and existence and non-singularity of the inverse transformation must be guaranteed. These conditions, translated in terms of the conformal and disformal functions, can be summarized as

$$A - 2BX > 0, \quad A(A - 2XB)(A - A_X X + 2B_X X^2) \neq 0, \quad (\text{A2})$$

for all values of ϕ and X .

The inverse of the barred metric $\bar{g}_{\mu\nu}$ is given by

$$\bar{g}^{\mu\nu} = \frac{1}{A} \left(g^{\mu\nu} - \frac{B}{A - 2BX} \phi^\mu \phi^\nu \right), \quad (\text{A3})$$

and the square root of the determinant of $\bar{g}_{\mu\nu}$ is related to the one of $g_{\mu\nu}$ as

$$\frac{\sqrt{-\bar{g}}}{\sqrt{-g}} = A^2 \sqrt{1 - \frac{2BX}{A}}. \quad (\text{A4})$$

One can easily derive the following relations between $g_{\mu\nu}$ and $\bar{g}_{\mu\nu}$:

$$\bar{\phi}^\mu = \bar{g}^{\mu\nu} \bar{\phi}_\nu = \frac{1}{A - 2BX} \phi^\mu, \quad (\text{A5})$$

$$\bar{X} = -\frac{1}{2} \bar{g}^{\mu\nu} \bar{\phi}_\mu \bar{\phi}_\nu = \frac{X}{A - 2BX}, \quad (\text{A6})$$

$$\frac{\partial \bar{g}_{\mu\nu}}{\partial g_{\alpha\beta}} = A \delta_\mu^\alpha \delta_\nu^\beta + \frac{1}{2} \left(A_X g_{\mu\nu} + B_X \phi_\mu \phi_\nu \right) \phi^\alpha \phi^\beta, \quad (\text{A7})$$

$$\frac{\partial g_{\mu\nu}}{\partial \bar{g}_{\alpha\beta}} = \frac{1}{A} \left[\delta_\mu^\alpha \delta_\nu^\beta - \frac{1}{2} C \left(A_X g_{\mu\nu} + B_X \phi_\mu \phi_\nu \right) \phi^\alpha \phi^\beta \right], \quad (\text{A8})$$

$$\frac{\partial \bar{g}_{\alpha\beta}}{\partial \phi_\mu} = B (\delta_\alpha^\mu \phi_\beta + \delta_\beta^\mu \phi_\alpha) - A_X g_{\alpha\beta} \phi^\mu - B_X \phi_\alpha \phi_\beta \phi^\mu, \quad (\text{A9})$$

$$C = \frac{1}{A - A_X X + 2B_X X^2}. \quad (\text{A10})$$

Also, one can define

$$\bar{T}_{(c)}^{\mu\nu} = \frac{2}{\sqrt{-\bar{g}}} \frac{\delta(\sqrt{-\bar{g}} \mathcal{L}_c)}{\delta \bar{g}_{\mu\nu}}, \quad (\text{A11})$$

corresponding to the energy-momentum tensor in the frame in which dark matter is minimally coupled to gravity. In such case, the pressure of dark matter in the old ($g_{\mu\nu}$) and new ($\bar{g}_{\mu\nu}$) frames are related through

$$T_{(c)}^{ij} = \sqrt{\frac{\bar{g}}{g}} \left[A \bar{T}^{ij} + \frac{1}{2} (A_X g_{\alpha\beta} + B_X \phi_\alpha \phi_\beta) \bar{T}_{(c)}^{\alpha\beta} \phi^i \phi^j \right], \quad (\text{A12})$$

Thus the pressureless property remains the same up to the linear order in a FLRW background.

Appendix B: Scale dependence of the mass term in the quasi-static limit

In Eq. (61) we have defined the scale dependent factor \mathcal{A} . For the canonical scalar field, Eq. (85), we have $\mathcal{A}_1 = 1$ and $m_\phi^2 = V_{\phi\phi}$, such that the scale dependence in the quasi-static limit appears as

$$\mathcal{A}(t, k) = \mathcal{A}_1 + \frac{a^2}{k^2} m_\phi^2 = 1 + \frac{a^2 H^2}{k^2} \frac{V_{\phi\phi}}{H^2}. \quad (\text{B1})$$

For sub-horizon scales, $k \gg aH$, as long as the ratio $V_{\phi\phi}/H^2$ is not too large, we can safely ignore the scale dependence.

In Fig. 16 we present the evolution of the ratio between the scalar mass, m_ϕ , and the Hubble parameter. In the uncoupled case, as well as for the conformal model II, the mass term is roughly the same order as the Hubble parameter during most part of the cosmic evolution. On the other hand, for model I the mass term is much smaller than H at early times, becoming of the same order around the present epoch. Hence, In both cases, the mass term can be safely ignored when the quasi-static limit is considered.

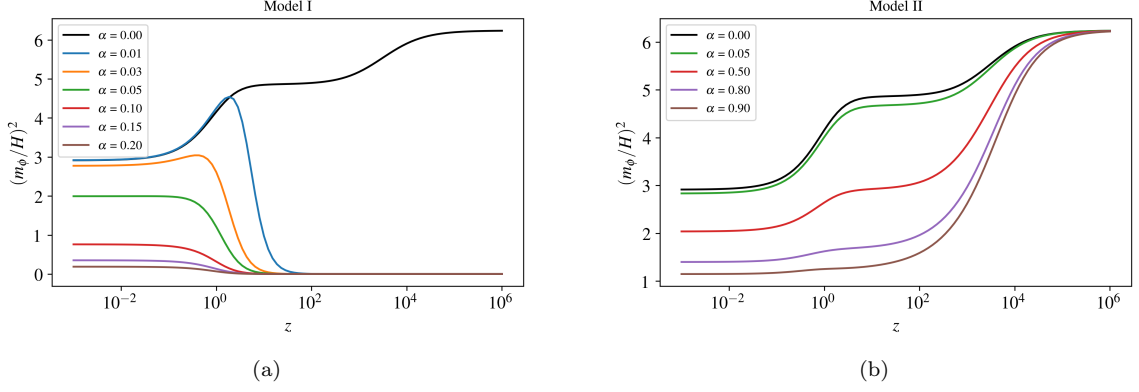


FIG. 16: Ratio between the m_ϕ^2 and H^2 in model I (left panel (a)) and model II (right panel (b)), as function of redshift for different values of the coupling constant.

Appendix C: Dispersion relation

In this Appendix, we investigate the dispersion relation of scalar perturbations. First of all, let us consider the conformal model I and II. In both cases, the coefficients (48) and (49) vanish, and therefore the gradient term in the perturbed equation for the scalar field (41) remains the same one as in quintessence case, implying the sound speed of the scalar perturbation is unity. Thus the sound horizon of scalar perturbation in both conformal models coincides with the cosmological horizon. On the other hand, the disformal model III has non-vanishing coefficients R_1 and R_2 , which modifies dispersion relation as we will see below.

The equation of motion for the perturbation of the canonical scalar field is

$$\delta\ddot{\phi} + 3H\delta\dot{\phi} + \left(\frac{k^2}{a^2} + V_{\phi\phi}\right)\delta\phi - \dot{\phi}(\dot{\Phi} + 3\dot{\Psi}) + 2V_\phi\Phi = -2Q_0\Phi - \delta Q. \quad (\text{C1})$$

In particular, for the disformal model III we have,

$$Q_0 = 0, \quad \delta Q = 2\alpha\frac{\rho_c}{\dot{\phi}^2}\frac{k^2}{a^2}(\dot{\phi}v_c - \delta\phi), \quad (\text{C2})$$

and since there is no anisotropic stress, $\Phi = \Psi$. Hence, Eq.(C1) becomes

$$\delta\ddot{\phi} + 3H\delta\dot{\phi} + \left[V_{\phi\phi} + \left(1 - 2\alpha\frac{\rho_c}{\dot{\phi}^2}\right)\frac{k^2}{a^2}\right]\delta\phi - 4\dot{\phi}\dot{\Psi} + 2V_\phi\Phi + 2\alpha\frac{\rho_c}{\dot{\phi}}\frac{k^2}{a^2}v_c = 0. \quad (\text{C3})$$

To compute the dispersion relation we need to express v_c in terms of $\delta\phi$, Ψ , and its time derivatives. But first, note that for model III the Euler equations, (57) and (59), lead to $\dot{v}_b = \dot{v}_c$, which means that since there is no coupling at background level, the velocity potentials will evolve in the same way. They will differ at most by a constant, $v_b = v_c + \text{constant}$. In what follows, we set this constant to zero. With that in mind, we use the $(0, i)$ component of Einstein equation, Eq. (35), to express the velocity as

$$(\rho_b + \rho_c)v_c = 2M_{\text{Pl}}^2(\dot{\Psi} + H\Psi) - \dot{\phi}\delta\phi, \quad (\text{C4})$$

Plugging this result into Eq. (C3), we arrive at

$$\delta\ddot{\phi} + \beta_1\delta\dot{\phi} + \left(\beta_2 + \gamma_2\frac{k^2}{a^2}\right)\delta\phi + \left(\beta_3 + \gamma_3\frac{k^2}{a^2}\right)\dot{\Psi} + \left(\beta_4 + \gamma_4\frac{k^2}{a^2}\right)\Psi = 0, \quad (\text{C5})$$

where,

$$\beta_1 = 3H, \quad \beta_2 = V_{\phi\phi}, \quad \beta_3 = -4\dot{\phi}, \quad \beta_4 = 2V_\phi, \quad (\text{C6})$$

$$\gamma_2 = 1 - 2\alpha\left(\frac{\rho_c}{\dot{\phi}^2} + \frac{\rho_c}{\rho_b + \rho_c}\right), \quad \gamma_3 = 4\alpha\frac{M_{\text{Pl}}^2\rho_c}{\dot{\phi}(\rho_b + \rho_c)}, \quad \gamma_4 = 4\alpha\frac{M_{\text{Pl}}^2H\rho_c}{\dot{\phi}(\rho_b + \rho_c)}. \quad (\text{C7})$$

To close the system, we use the (i, i) component of the Einstein equation, (36),

$$\ddot{\Psi} + \alpha_1 \dot{\Psi} + \alpha_2 \Psi + \alpha_3 \dot{\phi} + \alpha_4 \delta\phi = 0, \quad (\text{C8})$$

where the coefficients are given by

$$\alpha_1 = 4H, \quad \alpha_2 = 2\dot{H} + 3H^2 + \frac{\dot{\phi}^2}{2M_{\text{Pl}}^2}, \quad \alpha_3 = -\frac{\dot{\phi}}{2M_{\text{Pl}}^2}, \quad \alpha_4 = \frac{V_\phi}{2M_{\text{Pl}}^2}. \quad (\text{C9})$$

Assuming the time dependence $\delta\phi = e^{i\omega t}\delta\phi_0$ and $\Psi = e^{i\omega t}\Psi_0$, the system formed by Eqs. (C5) and (C8) admits solution if

$$\begin{vmatrix} -\omega^2 + i\alpha_1\omega + \alpha_2 & i\alpha_3\omega + \alpha_4 \\ i\left(\beta_3 + \gamma_3\frac{k^2}{a^2}\right)\omega + \beta_4 + \gamma_4\frac{k^2}{a^2} & -\omega^2 + i\beta_1\omega + \beta_2 + \gamma_2\frac{k^2}{a^2} \end{vmatrix} = 0. \quad (\text{C10})$$

For sub-horizon scales, $k^{-1} \ll (aH)^{-1}$, the coefficients α_i , β_i and γ_i are roughly constant within one Hubble time, and the large- k limit of the above expression yields,

$$\omega^2 \simeq (\gamma_2 - \alpha_3\gamma_3)k^2. \quad (\text{C11})$$

Hence, the sound velocity (group velocity) is given by

$$c_s^2 = \frac{\omega^2}{k^2} \simeq \gamma_2 - \alpha_3\gamma_3 = 1 - 2\alpha\frac{\rho_c}{\dot{\phi}^2}. \quad (\text{C12})$$

As expected, the sound speed for the uncoupled canonical scalar field is equal to unity. However, that is changed by the disformal coupling between dark matter and dark energy. The fact that c_s^2 must be positive leads to an upper bound for the coupling constant,

$$\alpha < \frac{\dot{\phi}^2}{2\rho_c}. \quad (\text{C13})$$

Furthermore, since during matter epoch $\Omega_c \ll \Omega_\phi$, we can approximate $\dot{\phi}^2/\rho_c \approx 0$, and a safer bound against instabilities is $\alpha < 0$.

The quasi-static approximation is valid for modes inside the sound horizon of scalar perturbations. For uncoupled quintessence, since the sound speed is equal to unity, the quasi-static limit is valid for all modes well inside the Hubble horizon. In the general case, one can define a sound horizon scale $k_s^{-1} = c_s(aH)^{-1}$, such that the quasi-static approximation is valid for modes satisfying $k \gg k_s$. For instance, in model III we require

$$k \gg \frac{aH}{\sqrt{1 - 2\alpha\frac{\rho_c}{\dot{\phi}^2}}}. \quad (\text{C14})$$

-
- [1] H. Gil-Marín, J. Noreña, L. Verde, W. J. Percival, C. Wagner, M. Manera, and D. P. Schneider, *Mon. Not. Roy. Astron. Soc.* **451**, 539 (2015), 1407.5668.
 - [2] S. More, H. Miyatake, R. Mandelbaum, M. Takada, D. Spergel, J. Brownstein, and D. P. Schneider, *Astrophys. J.* **806**, 2 (2015), 1407.1856.
 - [3] F. Zwicky, *Helvetica Physica Acta*, **6**, 110 (1933).
 - [4] H. W. Babcock, *Lick Observatory Bulletin* **19**, 41 (1939).
 - [5] F. D. Kahn and L. Woltjer, *ApJ* **130**, 705 (1959).
 - [6] D. Clowe, A. Gonzalez, and M. Markevitch, *Astrophys. J.* **604**, 596 (2004), astro-ph/0312273.
 - [7] S. Perlmutter et al. (Supernova Cosmology Project), *Bull. Am. Astron. Soc.* **29**, 1351 (1997), astro-ph/9812473.
 - [8] A. G. Riess et al. (Supernova Search Team), *Astron. J.* **116**, 1009 (1998), astro-ph/9805201.
 - [9] P. A. R. Ade et al. (Planck), *Astron. Astrophys.* **594**, A13 (2016), 1502.01589.
 - [10] I. Zlatev, L.-M. Wang, and P. J. Steinhardt, *Phys. Rev. Lett.* **82**, 896 (1999), astro-ph/9807002.
 - [11] T. Chiba, T. Okabe, and M. Yamaguchi, *Phys. Rev.* **D62**, 023511 (2000), astro-ph/9912463.
 - [12] C. Armendariz-Picon, V. F. Mukhanov, and P. J. Steinhardt, *Phys. Rev. Lett.* **85**, 4438 (2000), astro-ph/0004134.
 - [13] S. M. Carroll, V. Duvvuri, M. Trodden, and M. S. Turner, *Phys. Rev.* **D70**, 043528 (2004), astro-ph/0306438.

- [14] A. A. Starobinsky, *JETP Lett.* **86**, 157 (2007), 0706.2041.
- [15] W. Hu and I. Sawicki, *Phys. Rev.* **D76**, 064004 (2007), 0705.1158.
- [16] S. Capozziello, S. Carloni, and A. Troisi, *Recent Res. Dev. Astron. Astrophys.* **1**, 625 (2003), astro-ph/0303041.
- [17] G. W. Horndeski, *Int. J. Theor. Phys.* **10**, 363 (1974).
- [18] C. Deffayet, X. Gao, D. A. Steer, and G. Zahariade, *Phys. Rev.* **D84**, 064039 (2011), 1103.3260.
- [19] T. Kobayashi, M. Yamaguchi, and J. Yokoyama, *Prog. Theor. Phys.* **126**, 511 (2011), 1105.5723.
- [20] J. Gleyzes, D. Langlois, F. Piazza, and F. Vernizzi, *Phys. Rev. Lett.* **114**, 211101 (2015), 1404.6495.
- [21] D. Langlois and K. Noui, *JCAP* **1602**, 034 (2016), 1510.06930.
- [22] S. Tsujikawa, *Lect. Notes Phys.* **800**, 99 (2010), 1101.0191.
- [23] T. Clifton, P. G. Ferreira, A. Padilla, and C. Skordis, *Phys. Rept.* **513**, 1 (2012), 1106.2476.
- [24] J. D. Bekenstein, *Phys. Rev.* **D48**, 3641 (1993), gr-qc/9211017.
- [25] J. Ben Achour, D. Langlois, and K. Noui, *Phys. Rev.* **D93**, 124005 (2016), 1602.08398.
- [26] J.-P. Uzan, *Rev. Mod. Phys.* **75**, 403 (2003), hep-ph/0205340.
- [27] D. J. Kapner, T. S. Cook, E. G. Adelberger, J. H. Gundlach, B. R. Heckel, C. D. Hoyle, and H. E. Swanson, *Phys. Rev. Lett.* **98**, 021101 (2007), hep-ph/0611184.
- [28] J. Khoury and A. Weltman, *Phys. Rev. Lett.* **93**, 171104 (2004), astro-ph/0309300.
- [29] L. Hui, A. Nicolis, and C. Stubbs, *Phys. Rev.* **D80**, 104002 (2009), 0905.2966.
- [30] G. Dvali, *New J. Phys.* **8**, 326 (2006), hep-th/0610013.
- [31] A. Joyce, B. Jain, J. Khoury, and M. Trodden, *Phys. Rept.* **568**, 1 (2015), 1407.0059.
- [32] B. Wang, E. Abdalla, F. Atrio-Barandela, and D. Pavon, *Rept. Prog. Phys.* **79**, 096901 (2016), 1603.08299.
- [33] N. Kaiser, *Mon. Not. Roy. Astron. Soc.* **227**, 1 (1987).
- [34] M. Takada, R. S. Ellis, M. Chiba, J. E. Greene, H. Aihara, N. Arimoto, K. Bundy, J. Cohen, O. Doré, G. Graves, et al., *Publications of the Astronomical Society of Japan* **66**, R1 (2014), 1206.0737.
- [35] T. Delubac et al., *Mon. Not. Roy. Astron. Soc.* **465**, 1831 (2017), 1611.06934.
- [36] G. D. Racca, R. Laureijs, L. Stagnaro, J.-C. Salvignol, J. Lorenzo Alvarez, G. Saavedra Criado, L. Gaspar Venancio, A. Short, P. Strada, T. Bönke, et al., in *Space Telescopes and Instrumentation 2016: Optical, Infrared, and Millimeter Wave* (2016), vol. 9904, p. 990400, 1610.05508.
- [37] D. Spergel, N. Gehrels, C. Baltay, D. Bennett, J. Breckinridge, M. Donahue, A. Dressler, B. S. Gaudi, T. Greene, O. Guyon, et al., *ArXiv e-prints* (2015), 1503.03757.
- [38] R. Maartens, F. B. Abdalla, M. Jarvis, and M. G. Santos, *PoS AASKA14*, 016 (2015), 1501.04076.
- [39] D. J. Bacon and others (SKA Cosmology SWG) (2018), 1811.02743.
- [40] D. Yamauchi et al., *Publ. Astron. Soc. Jap.* **68**, R2 (2016), 1603.01959.
- [41] N. Aghanim et al. (Planck) (2018), 1807.06209.
- [42] R. Kimura, T. Suyama, M. Yamaguchi, D. Yamauchi, and S. Yokoyama, *Publ. Astron. Soc. Jap.* **70**, Publications of the Astronomical Society of Japan, Volume 70, Issue 5, 1 October 2018, L5, <https://doi.org/10.1093/pasj/psy083> (2018), 1709.09371.
- [43] J. Gleyzes, D. Langlois, M. Mancarella, and F. Vernizzi, *JCAP* **1602**, 056 (2016), 1509.02191.
- [44] I. Sawicki and E. Bellini, *Phys. Rev.* **D92**, 084061 (2015), 1503.06831.
- [45] A. Elia, A. D. Ludlow, and C. Porciani, *Mon. Not. Roy. Astron. Soc.* **421**, 3472 (2012), 1111.4211.
- [46] I. Hashimoto, A. Taruya, T. Matsubara, T. Namikawa, and S. Yokoyama, *Phys. Rev.* **D93**, 103537 (2016), 1512.08352.
- [47] B. Ratra and P. J. E. Peebles, *Phys. Rev.* **D37**, 3406 (1988).
- [48] R. R. Caldwell, R. Dave, and P. J. Steinhardt, *Phys. Rev. Lett.* **80**, 1582 (1998), astro-ph/9708069.
- [49] R. R. Caldwell and E. V. Linder, *Phys. Rev. Lett.* **95**, 141301 (2005), astro-ph/0505494.
- [50] P. J. Steinhardt, L.-M. Wang, and I. Zlatev, *Phys. Rev.* **D59**, 123504 (1999), astro-ph/9812313.
- [51] S. Weinberg, *Cosmology* (Oxford University Press, Oxford New York, 2008), ISBN 978-0198526827.
- [52] D. Blas, J. Lesgourgues, and T. Tram, *JCAP* **1107**, 034 (2011), 1104.2933.
- [53] L. Amendola, *Phys. Rev.* **D62**, 043511 (2000), astro-ph/9908023.
- [54] L. Amendola, *Phys. Rev. Lett.* **86**, 196 (2001), astro-ph/0006300.
- [55] X. Zhang, *Phys. Lett.* **B611**, 1 (2005), astro-ph/0503075.
- [56] L. Amendola, M. Baldi, and C. Wetterich, *Phys. Rev.* **D78**, 023015 (2008), 0706.3064.
- [57] M. Tegmark, *Phys. Rev. Lett.* **79**, 3806 (1997), astro-ph/9706198.
- [58] H.-J. Seo and D. J. Eisenstein, *Astrophys. J.* **598**, 720 (2003), astro-ph/0307460.
- [59] C. Alcock and B. Paczynski, *Nature* **281**, 358 (1979).
- [60] M. White, Y.-S. Song, and W. J. Percival, *Mon. Not. Roy. Astron. Soc.* **397**, 1348 (2008), 0810.1518.
- [61] P. A. R. Ade et al. (Planck), *Astron. Astrophys.* **594**, A14 (2016), 1502.01590.
- [62] C. Li, Y. P. Jing, G. Kauffmann, G. Boerner, X. Kang, and L. Wang, *Mon. Not. Roy. Astron. Soc.* **376**, 984 (2007), astro-ph/0701218.
- [63] P. Bull, P. G. Ferreira, P. Patel, and M. G. Santos, *Astrophys. J.* **803**, 21 (2015), 1405.1452.
- [64] L. Amendola et al. (2016), 1606.00180.
- [65] S. Yahya, P. Bull, M. G. Santos, M. Silva, R. Maartens, P. Okouma, and B. Bassett, *Mon. Not. Roy. Astron. Soc.* **450**, 2251 (2015), 1412.4700.
- [66] R. E. Smith, J. A. Peacock, A. Jenkins, S. D. M. White, C. S. Frenk, F. R. Pearce, P. A. Thomas, G. Efstathiou, and H. M. P. Couchmann (VIRGO Consortium), *Mon. Not. Roy. Astron. Soc.* **341**, 1311 (2003), astro-ph/0207664.

[67] T. Sprenger, M. Archidiacono, T. Brinckmann, S. Clesse, and J. Lesgourgues (2018), 1801.08331.